



Article

Biochemical and Physical Characterization of Immobilized *Candida rugosa* Lipase on Metal Oxide Hybrid Support

Nurfadhila Nasya Ramlee¹, Rosli Md Illias^{1,2}, Roshanida A. Rahman^{1,2}, Susilawati Toemen³ , Rangabhashiyam Selvasembian⁴, Rabi'atul Adawiyah Ahmad⁵ , Nor Hasmaliana Abdul Manas^{1,2} and Nur Izyan Wan Azelee^{1,2,*}

¹ School of Chemical and Energy Engineering, Faculty of Engineering, Universiti Teknologi Malaysia, Skudai 81310, Johor, Malaysia; nurfadhilanasya24@gmail.com (N.N.R.); r-rosli@utm.my (R.M.I.); r-anida@utm.my (R.A.R.); hasmaliana@utm.my (N.H.A.M.)

² Institute of Bioproduct Development (IBD), Universiti Teknologi Malaysia, Skudai 81310, Johor, Malaysia

³ Department of Chemistry, Faculty of Science, Universiti Teknologi Malaysia, Skudai 81310, Johor, Malaysia; susilawatitoemen@utm.my

⁴ Department of Biotechnology, School of Chemical and Biotechnology, SASTRA Deemed University, Thanjavur 613401, Tamil Nadu, India; rambhashiyam@gmail.com

⁵ School of Life Science, Faculty of Health and Life Sciences, INTI International University,

Persiaran Perdana BBN Putra Nilai, Nilai 71800, Negeri Sembilan, Malaysia; rabiatal.ahmad@newinti.edu.my

* Correspondence: nur.izyan@utm.my; Tel.: +6013-7975900

Abstract: Enzyme immobilization on inorganic materials is gaining more attention with the potential characteristics of high-surface-area-to-volume ratios, increasing the efficiency of enzyme loading on the support. Metal oxide hybrid support was prepared by a wetness impregnation of five metal precursors, including CaO, CuO, MgO, NiO, and ZnO, on Al₂O₃ and used as a support for the immobilization of *Candida rugosa* lipase (CRL) by adsorption. Maximum activity recovery (70.6%) and immobilization efficiency (63.2%) were obtained after optimization of five parameters using response surface methodology (RSM) by Box–Behnken design (BBD). The biochemical properties of immobilized CRL showed high thermostability up to 70 °C and a wide range in pH stability (pH 4–10). TGA-DTA and FTIR analysis were conducted, verifying thermo-decomposition of lipase and the presence of an amide bond. FESEM-EDX showed the homogeneous distribution and high dispersion of magnesium and CRL on MgO–Al₂O₃, while a nitrogen adsorption–desorption study confirmed MgO–Al₂O₃ as a mesoporous material. CRL/MgO–Al₂O₃ can be reused for up to 12 cycles and it demonstrated high tolerance in solvents (ethanol, isopropanol, methanol, and tert-butanol) compared to free CRL.

Keywords: magnesium oxide; *Candida rugosa* lipase; wetness impregnation; enzyme immobilization; response surface methodology (RSM); biodiesel



Citation: Ramlee, N.N.; Md Illias, R.; A. Rahman, R.; Toemen, S.; Selvasembian, R.; Ahmad, R.A.; Abdul Manas, N.H.; Wan Azelee, N.I. Biochemical and Physical Characterization of Immobilized *Candida rugosa* Lipase on Metal Oxide Hybrid Support. *Catalysts* **2022**, *12*, 854. <https://doi.org/10.3390/catal12080854>

Academic Editors: Qinghua Lai, Qingfeng Zhang and Run-Ping Ye

Received: 10 July 2022

Accepted: 1 August 2022

Published: 3 August 2022

Publisher's Note: MDPI stays neutral with regard to jurisdictional claims in published maps and institutional affiliations.



Copyright: © 2022 by the authors. Licensee MDPI, Basel, Switzerland. This article is an open access article distributed under the terms and conditions of the Creative Commons Attribution (CC BY) license (<https://creativecommons.org/licenses/by/4.0/>).

1. Introduction

Lipases are known as versatile enzymes, owing to their ability to catalyze many reactions, such as hydrolysis, alcoholysis, esterification, transesterification, acidolysis, aminolysis, and amidation [1,2]. The stability and flexibility of lipase to catalyze these reactions, as well as having a wide range in substrate specificity, make it highly attractive from a commercial perspective. The application of lipases has been explored for the synthesis of aromatic flavor esters [3], detergent [4], degreasing fats in the leather industry [5], treatment of fat-containing waste effluents [6], biodiesel production [7], simultaneous transesterification–esterification [8], and many more. Despite numerous advantages, free enzymes have low tolerance in organic solvents, are expensive, and are not economically promising. Lipase immobilization on solid supports has gained remarkable attention to overcome the limitations of homogeneously catalyzed processes. The immobilization methods have been employed to improve lipase stability in organic solvents, reproducibility, and

make product recovery much easier [9]. Conventional immobilization, such as adsorption via hydrogen bonding, electrostatic interaction, hydrophobic interaction, Van der Waals forces, and ionic interaction, is still gaining lots of attention, despite the development of advanced and sophisticated methods. However, the disadvantage of this technique is enzyme leaching due to weak binding between enzyme and support. Among these interactions, the immobilization of lipase via ionic interactions is gaining lots of attention because it provides strong interaction between the opposite charge on the support and amino group of the lipase, but still allowing support regeneration by incubating the immobilized lipase at ionic detergents [10]. Nazzoly Rueda et al. [10] synthesized octyl-glutamic heterofunctional agarose beads with hydrophobic properties and the presence of two anionic groups and one cationic group, allowing lipase immobilization via interfacial activation and ionic interaction with anionic amino group of the lipases. Sabi et al. [11] reported that the adsorption process of lipase on silica may occur via ionic interactions in negatively charged silanol groups ($-\text{Si}-\text{O}^-$), with positive groups of lysine or arginine residues ($-\text{NH}_3^+$) of *Thermomyces lanuginosus* lipase. In addition, amino acids can be used to tailor the surface of the support, resulting in the changes in the charge density of the support [12]. Hence, the selection of support materials and their surface charges is becoming one of the crucial things to consider for enzyme immobilization via ionic interaction.

Aluminum oxide (Al_2O_3), also known as alumina, is inorganic support that plays a crucial role in industries. Thanks to its excellent properties, such as good thermal stability, high mechanical resistance [13], good catalytic activity [14], high porosity, and large surface area, it can provide high dispersion of the active metal species [15]. These properties act as a major attraction from a catalytic or adsorption point of view. The surface properties of Al_2O_3 can be altered by the addition of metallic species, which can change the isoelectric point (pI) of the Al_2O_3 , hence, increasing the electrostatic interaction between enzyme and the support [16]. The modification of hydroxyapatite with metal ions (Cu^{2+} and Ni^{2+}) showed efficient immobilization of xylanase due to coordination interactions between metal ions on the support surface and electron donor groups on the enzyme surface [17]. Wang et al. [18] found that the pH of solution can change the pI of MgO and resulted in significant effects on the adsorption and decomposition of ozone. Another study, conducted by Mulcahy et al. [19], showed that the addition of different concentrations of fluoride on Al_2O_3 resulted in changes in pI and affected the adsorption capacity of molybdates on the support. In addition to that, several types of metal oxide (TiO_2 and ZrO_2) have been studied for β -galactosidase immobilization by tailoring its pI and surface area [20]. Despite the variety of methods that have been established, the wetness impregnation method is the easiest and least expensive method to add metal oxide on the support [21].

Commonly, the catalysts for biodiesel production are derived from chemical (acid/alkali) or biological sources (enzymes). The chemically catalyzed transesterification using an acid or alkali catalyst gives high conversion of triglycerides to methyl esters in a short reaction time. However, the use of chemically catalyzed transesterification has several limitations, especially in cost effectiveness, due to high temperatures, leading to energy intensity, requirement for low-free-fatty-acid content [22], extensive separation process [22], wastewater generation, and leaching of the catalyst [23]. Lipase-mediated transesterification can be carried out under mild reaction conditions to produce high-quality biodiesel that is free of contaminants, favoring an easy recovery of glycerol, without the need for purification or chemical waste release [24]. In addition, the application of enzymes may eliminate the deacidification or esterification process prior to transesterification reaction and reduce the quantities of hazardous solvents needed, thus, making the process cost effective and environmentally friendly [25]. However, the reaction time using an enzymatic catalyst is longer compared to using a chemical catalyst [26]. By virtue of these issues, this paper presents a preparation of magnesium oxide (MgO) impregnated on aluminum oxide (Al_2O_3) that serves as a support for lipase immobilization and as a chemical catalyst for biodiesel production. *Candida rugosa* lipase (CRL) was chosen as a model enzyme due to

nonspecific activity, which can transesterify all the ester bonds of triglycerides and esterify them in the presence of alcohols.

The synthesis of heterogeneous chemical catalysts and development of immobilized lipase have gained outstanding attention for biodiesel production. Recently, the immobilization of lipase on metal organic frameworks via adsorption for biodiesel production was studied by Le Zhong et al. [27]. Meanwhile, a previous study conducted by Ashok et al. [28] shows that MgO has the catalytic activity to perform a transesterification reaction. This study is the first report on the application of a chemoenzymatic catalyst for biodiesel production, combining MgO and lipase as a chemical and enzymatic catalyst on a single support. Hence, in this study, the screening of five types of metal oxide, the optimization of CRL immobilization on metal hybrid support, and its characterization were performed for further application as a chemoenzymatic catalyst for biodiesel production. A rigorous and systematic investigation on the effects of MgO addition on the immobilization efficiency, activity recovery, biochemical and chemical characterization of the free CRL, and the immobilized CRL on MgO-Al₂O₃ (CRL/MgO-Al₂O₃) were evaluated in this study. CRL/MgO-Al₂O₃ was investigated to demonstrate high recyclability of the enzyme and high solvent tolerance, which is impossible to achieve using free CRL. Lastly, the prepared catalysts are employed for transesterification reaction for biodiesel production. This study was conducted to further expand the prospects of enzyme immobilization towards metal hybrid support as well as its ability to perform a transesterification reaction of high acid value of waste cooking oil for biodiesel production.

2. Results and Discussion

2.1. Effect of Metal Oxides Ratio to Al₂O₃ for Wetness Impregnation Method

Lipase immobilization performances on five types of MO-Al₂O₃ was measured in terms of activity recovery of the adsorbed enzymes. Three types of metal oxide were chosen to be studied in this research: alkaline earth metal oxide (CaO and MgO), post-transition metal oxide (ZnO), and transition metal oxide (NiO and CuO). The results presented in Figure 1 show the effect of MO ratio to Al₂O₃ towards activity recovery. The MO ratio to Al₂O₃ was 0.05–0.25 (*w/w*) for MgO, ZnO, and NiO, while 0.25–1.5 (*w/w*) % for CaO and CuO.

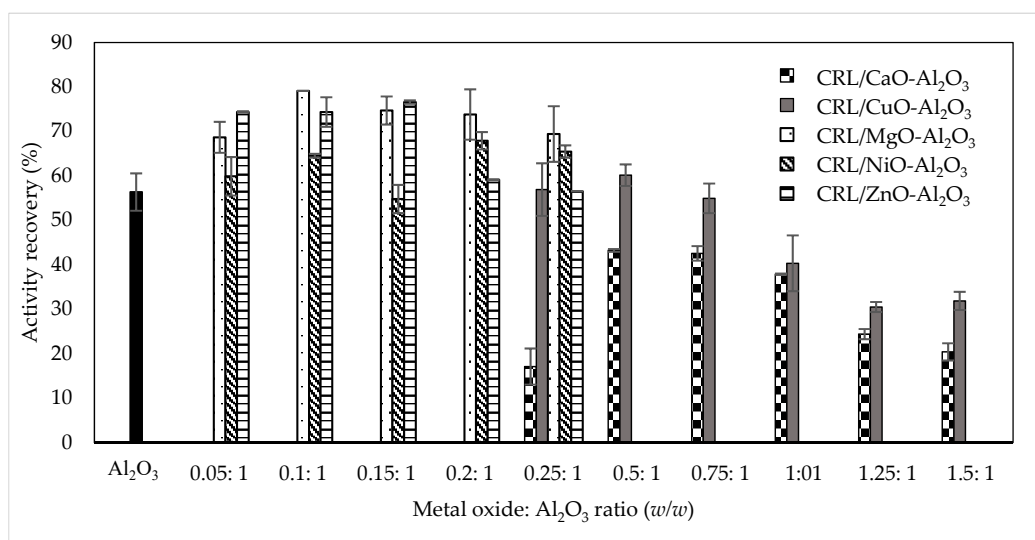


Figure 1. Effect of MO: Al₂O₃ ratio on activity recovery.

In the alkaline earth metal oxide group, the activity recovery for CRL immobilized on MgO was higher than CaO when using 0.1:1 *w/w* of MgO: Al₂O₃ ratio and 0.5:1 *w/w* of CaO: Al₂O₃ resulting in 79.11% and 43.22% of activity recovery, respectively. For the transition metal oxide group, 0.2:1 *w/w* of NiO: Al₂O₃ ratio gave the highest activity recovery of

67.88%, which is higher compared to 0.5: 1 *w/w* of CuO: Al₂O₃ with 60.18% activity recovery. Meanwhile, for the post-transition metal oxide group, 0.15:1 *w/w* ratio of ZnO: Al₂O₃ presented 76.59% of activity recovery. In general, the addition of metal oxides on Al₂O₃ increased the activity recovery of immobilized CRL as compared to immobilization on Al₂O₃, except for CaO, which showed a 0.77-fold decrement in activity recovery. The highest activity recovery was observed when using MgO, with a 1.4-fold increment in activity recovery, followed by ZnO, NiO, and CuO with 1.36, 1.21, and 1.07, respectively. The performance of the metal oxides for CRL immobilization was evaluated in ascending order starting from CaO < Al₂O₃ < CuO < NiO < ZnO < MgO.

Previously, γ -Al₂O₃, MgO, and ZnO were used for the immobilization of β -galactosidase via a simple adsorption mechanism. γ -Al₂O₃ shows the highest activity of 268 U/g, while no activity was detected for MgO and ZnO [20]. Interestingly, our result shows a contradiction with previous findings by Satyawali et al. (2013). This study showed high-activity recovery for MgO (79.11%) and ZnO (76.59%), while low-activity recovery for Al₂O₃ (56.33%). This could be attributed to the type of enzyme used in our study, lipase from *Candida rugosa*. Possibly, the enzyme was bound to the Al₂O₃ with its active site and lost its biocatalytic activity. It can be seen that the metal-oxide-to-Al₂O₃ ratio is one of the important parameters affecting activity recovery of the immobilized enzymes, probably due to an alteration in surface charge that affects the adsorption of enzymes on the support. Hence, 0.1:1 *w/w* of MgO: Al₂O₃, 0.5:1 *w/w* of CaO: Al₂O₃, 0.2:1 *w/w* of NiO: Al₂O₃, 0.5: 1 *w/w* of CuO: Al₂O₃, and 0.15:1 *w/w* ratio of ZnO: Al₂O₃ were chosen for screening at different calcination temperatures, attributed to high-activity recovery.

2.2. Effect of Calcination Temperature

All the metal oxides were subjected to calcination at 300–700 °C and immobilization performance was evaluated through activity recovery of CRL, as presented in Figure 2. Varying calcination temperature is one of the approaches to study the dispersion of metal on the support and tailoring the surface area and basicity of the support [29]. As evident from the results, five different types of metal oxides show different activity recovery at different calcination temperatures. Increasing the calcination temperature in Al₂O₃ from 300 to 400 °C shows an increment in activity recovery from 56.33 to 71.40%, respectively. Meanwhile, for CRL/CaO-Al₂O₃, varying calcination temperature from 300–400 °C shows a significant increase in activity recovery from 43.22% to 67.40%. A further increment in calcination temperature at 700 °C declined the activity recovery up to 2.47% due to reduction in surface area caused by sintering of fine crystals and cluster aggregation [30].

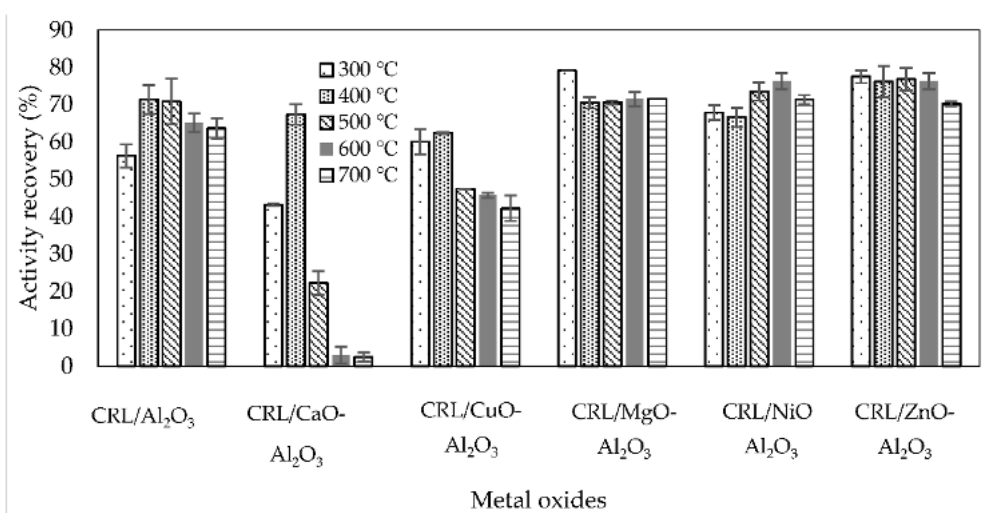


Figure 2. Effect of different calcination temperatures of MO-Al₂O₃ towards activity recovery.

CRL/MgO-Al₂O₃ showed the highest activity recovery obtained of 79.11%, when calcined at 300 °C. After 500 °C, the activity recovery dropped, resulting from the lost hydroxyl groups on temperature treatment, thus, decreasing enzyme immobilization on the support. In the case of CRL/ZnO-Al₂O₃, no significant difference was observed by varying calcination temperature, yielding 70.34% in the lowest activity recovery when calcined at 700 °C. In addition, the highest activity recovery for CRL/NiO-Al₂O₃ was 76.31% when the carrier was calcined at 600 °C and decreased afterwards. Because of the weak interaction between NiO and Al₂O₃ as the calcination temperature increased, there was more free Ni on the support surface and the Ni was more likely to migrate and aggregate, resulting in a decrease in adsorption capacity of CRL [29]. For CRL/CuO-Al₂O₃, activity recovery for immobilized CRL increased when the support was calcined at 400 °C, resulting in 62.45% of activity recovery and the trend for activity recovery decreased when calcined > 400 °C. These results suggest that the calcination temperature changes the physiochemical properties of the MO-Al₂O₃ and affects the activity recovery of the immobilized CRL. Based on the obtained results on activity recovery of immobilized lipase, 0.1:1 *w/w* of MgO: Al₂O₃ ratio, calcined at 300 °C, was selected for optimization of CRL immobilization.

2.3. Optimization of CRL Immobilization Using RSM for Activity Recovery

The optimization of immobilization parameters was performed using Box–Behnken Design (BBD). The coded values, experimental, and predicted values for activity recovery and immobilization yield are given in Table 1.

Table 1. Experimental design for response surface design for CRL immobilization on MgO-Al₂O₃ using BBD.

Run Order	Agitation Speed (rpm)	CRL Concentration (g/L)	Temperature (°C)	Immobilization Time (hour)	Weight of MgO-Al ₂ O ₃ Beads (g)	Activity Recovery (%)		Immobilization Efficiency (%)	
						Experimental Value	Predicted Value	Experimental Value	Predicted Value
1	100	2.5	30	6	3	64.7	65.0	44.6	43.2
2	100	1	30	4	1	48.6	45.3	57.3	57.2
3	100	2.5	20	6	2	67.7	68.1	30.8	30.4
4	100	2.5	30	6	1	54.6	59.1	40.1	38.7
5	150	2.5	30	6	2	73.6	71.0	39.9	38.1
6	100	2.5	20	2	2	62.5	66.2	21.6	20.6
7	50	2.5	20	4	2	57.5	58.2	24.2	22.0
8	100	2.5	30	2	3	65.5	63.1	55.6	56.6
9	150	2.5	30	2	2	70.6	69.0	17.1	17.1
10	100	4	30	2	2	70.6	73.0	34.9	33.3
11	100	1	40	4	2	43.4	42.1	50.6	47.1
12	100	2.5	20	4	3	64.0	70.1	47.2	48.5
13	100	2.5	20	4	1	63.3	64.2	27.2	28.3
14	100	2.5	30	4	2	60.9	61.1	73.0	73.9
15	100	1	30	4	3	50.7	51.1	80.5	81.0
16	150	2.5	30	4	3	76.6	72.9	51.6	50.1
17	50	1	30	4	2	40.5	39.3	62.6	68.4
18	100	2.5	40	4	3	55.2	57.9	40.8	42.3
19	100	2.5	30	2	1	60.8	57.2	28.0	28.9
20	50	2.5	30	2	2	52.0	51.2	45.0	47.4
21	150	1	30	4	2	54.3	57.1	45.7	48.7
22	150	2.5	20	4	2	78.0	76.1	32.0	33.8
23	150	2.5	40	4	2	57.1	63.9	11.8	12.4
24	100	4	30	6	2	78.4	74.9	14.9	16.9
25	100	2.5	40	4	1	52.2	52.1	29.1	30.4
26	100	2.5	40	2	2	52.4	54.1	27.8	30.1
27	100	2.5	30	4	2	63.4	61.1	73.3	73.9
28	100	4	40	4	2	67.9	67.9	24.7	23.1
29	50	2.5	30	4	1	44.3	49.2	43.0	41.5
30	100	1	30	2	2	50.6	47.2	53.7	49.8
31	100	2.5	30	4	2	61.4	61.1	75.5	73.9

Table 1. Cont.

Run Order	Agitation Speed (rpm)	CRL Concentration (g/L)	Temperature (°C)	Immobilization Time (hour)	Weight of MgO-Al ₂ O ₃ Beads (g)	Activity Recovery (%)		Immobilization Efficiency (%)	
						Experimental Value	Predicted Value	Experimental Value	Predicted Value
32	150	4	30	4	2	84.3	82.9	31.5	29.8
33	50	2.5	40	4	2	47.4	46.1	42.7	39.2
34	150	2.5	30	4	1	66.4	67.1	31.5	30.9
35	50	2.5	30	6	2	54.3	53.1	22.2	22.8
36	100	1	30	6	2	49.6	49.2	63.0	62.6
37	50	2.5	30	4	3	54.1	55.1	57.0	54.5
38	100	1	20	4	2	53.7	54.3	57.6	56.3
39	50	4	30	4	2	68.2	65.0	24.1	25.1
40	100	4	30	4	1	69.3	71.0	33.5	33.8
41	100	4	20	4	2	83.2	80.0	17.6	18.1
42	100	2.5	40	6	2	57.2	56.0	14.1	16.8
43	100	4	30	4	3	75.6	76.9	41.2	42.2

Among the 43 experimental runs, including replicates, run number 32 shows the highest activity recovery (84.3%), while run number 17 shows the lowest activity recovery of 40.5%. The subsequent analysis of variance (ANOVA) for activity recovery is shown in Table 2. Activity recovery is most suitably described with a linear model following Equation (1).

$$Y = 61.07 + 8.92 A + 12.88 B - 6.06 C + 0.96 D + 2.92 E \quad (1)$$

Table 2. Analysis of variance (ANOVA) and fit statistics of the linear model for activity recovery response.

Source	Sum of Squares	df	Mean Square	F-Value	p-Value	
Model	4667.27	5	933.5	118.69	<0.0001	significant
A-Agitation speed	1272.42	1	1272.42	161.79	<0.0001	
B-CRL concentration	2655.22	1	2655.22	337.61	<0.0001	
C-Temperature	587.62	1	587.62	74.71	<0.0001	
D-Time	14.68	1	14.68	1.87	0.1802	
E-Weight of beads	137.33	1	137.33	17.46	0.0002	
Residual	291	37	7.86			
Lack of Fit	287.7	35	8.22	4.98	0.1811	not significant
Pure Error	3.3	2	1.65			
Cor Total	4958.27	42				
Standard deviation	2.80			R ²	0.9413	
Mean	61.07			Adjusted R ²	0.9334	
C.V.%	4.59			Predicted R ²	0.9195	
Adequate precision	41.62					

The model expressed by Equation (1) represents activity recovery (Y) as a function of agitation speed (A), CRL concentration (B), temperature (C), time (D), and weight of MgO-Al₂O₃ beads (E). A positive sign in front of the terms indicates a synergistic effect in increasing activity recovery, whereas a negative sign indicates an antagonistic effect [31]. The F-test for ANOVA was performed to determine the model's statistical significance. The regression is statistically significant at the 95 percent confidence level if the p (<0.0001) of the model in the F-test is very low [32]. There is barely a 0.01 percent risk that noise will cause a model failure. The p-value for the term 'lack of fit', which is an evaluation to determine the impact of disparities between the actual and predicted values on the pure error among replicates, was 0.1811, which is more than 0.05 and indicates that the p-value is not significant. Furthermore, the F-value of 4.98 for 'lack of fit' indicates that the lack of fit is not significant in comparison to the pure error. Due to noise, a significant lack-of-fit

F-value has an 18.11 percent chance of occurring. The correlation measure to determine the quality of the model is through evaluation of the coefficient of determination (R^2). The obtained R^2 was 0.9413, indicating that 94 percent of the experimental data are consistent with the model's data. The adjusted R^2 reached a high of 0.9334, indicating the model's importance. Meanwhile, the models' high anticipated R^2 suggested that the experimental data and theoretical values predicted by the model were in close agreement.

Figure 3A–E shows the effect of agitation speed, CRL concentration, temperature, immobilization time, and weight of MgO-Al₂O₃ toward activity recovery. Based on the result of regression coefficients, an increment value of agitation speed from 50 to 150 rpm (Figure 3A) and CRL concentration from 2 to 4 g/L (Figure 3B) resulted in increased activity recovery. The non-uniform distribution of the enzyme in the immobilization mixture during the adsorption process can be linked to the low immobilization yield at 50 rpm of agitation speed, resulting in low-activity recovery [33]. Meanwhile, the increment in CRL loading provides more enzymes to be adsorbed on the support, resulting in high-activity recovery. On the contrary, Figure 3C portrayed that a rise in temperature, from a low level (20 °C) to a high level (40 °C), shows a decrement in activity recovery due to a reduction in non-specific binding of the lipase on the MgO-Al₂O₃ support, which changed the structure of the enzyme and made it susceptible to thermal degradation [34]. Another study reported that thermal inactivation of lipase occurred after 30 °C [35]. In addition, varying the immobilization time from 2 to 6 h, as shown in Figure 3D, did not show significant difference towards activity recovery due to *p*-value > 0.05. The results obtained come to an agreement with a study conducted by Adnan et al., reporting that the immobilization of lipase was not affected by prolonging the immobilization time [35]. Meanwhile, the increment in weight of MgO-Al₂O₃ beads shows an increment in activity recovery (Figure 3E) because more space is provided for the enzyme to be immobilized and can prevent the enzyme crowding effect. A linear model demonstrates that the interaction between five parameters during the immobilization treatment has no significant effect on activity recovery. The interaction between parameters during the immobilization operation, on the other hand, can be detected in terms of immobilization efficiency.

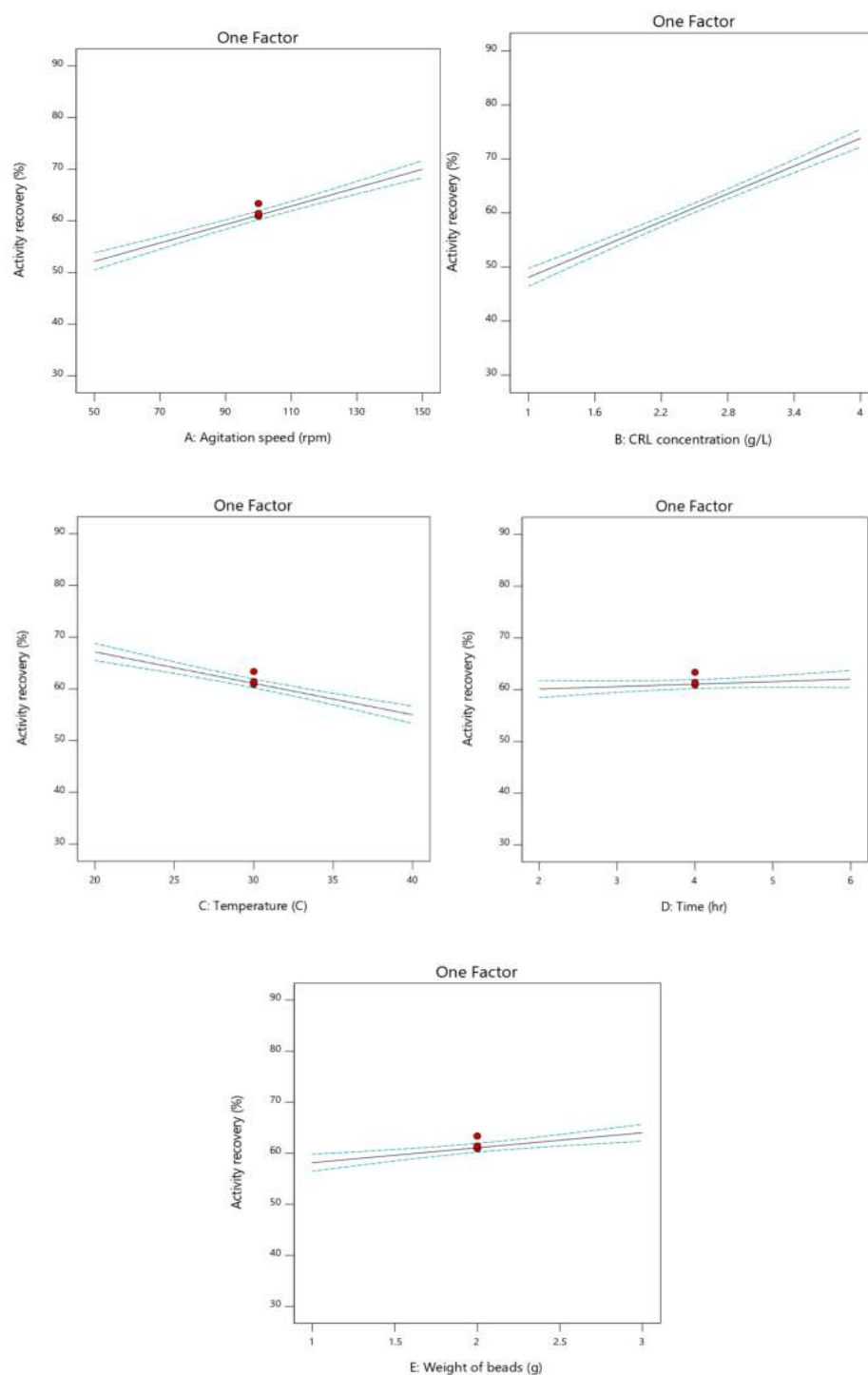


Figure 3. One-factor effect of five independent variables: (A) agitation speed, (B) CRL concentration (g/L), (C) temperature, (D) time, and (E) weight of MgO-Al₂O₃ beads towards activity recovery.

2.4. Optimization of CRL Immobilization Using RSM for Immobilization Efficiency

Table 3 shows that the second-order polynomial model has an R^2 value of 0.9882, indicating a strong correlation between the theoretical values predicted by the model and the experimental results. The second-order polynomial model was chosen to study the interaction of two different parameters on the same response. The immobilization efficiency and the process variables of agitation speed (rpm), CRL concentration (g/L), temperature (°C), time (hour), and weight of MgO-Al₂O₃ beads are linked by a second-order polynomial regression equation (g). When the response surface has a curvature, the first-order model is

insufficient. As a result, the second-order model is beneficial for approximating the section of the true response surface with curvature, as well as being very significant and sufficient to describe the actual relationship between the response and the five parameters. Based on the ANOVA results, the factors, and their interactions, a p -value lower than 0.05 (95% level) was considered statistically significant in model terms. Therefore, according to Table 3, A, B, E, AB, AC, AD, BC, BD, BE, CD, DE, A^2 , B^2 , C^2 , D^2 , and E^2 are significant model terms (p -value < 0.0001) and the suggested model is significant (p < 0.05). Model F -value of 92.08 implies the model is significant and there is only a 0.01% chance that an F -value could occur due to noise. The predicted R^2 of 0.9533 is in reasonable agreement with the adjusted R^2 (0.9755), thus, acknowledging the validity of the model. Therefore, this model is adequate to predict the immobilization results within the range of the variables.

Table 3. ANOVA and fit statistics of the quadratic model for immobilization efficiency.

Source	Sum of Squares	df	Mean Square	F -Value	p -Value	
Model	13,152.38	20	657.62	92.08	<0.0001	significant
A-Agitation speed	224.05	1	224.05	31.37	<0.0001	
B-CRL concentration	3866.35	1	3866.35	541.38	<0.0001	
C-Temperature	17.24	1	17.24	2.41	0.1345	
D-Time	12.54	1	12.54	1.76	0.1987	
E-Weight of beads	1037.16	1	1037.16	145.23	<0.0001	
AB	147.14	1	147.14	20.60	0.0002	
AC	373.43	1	373.43	52.29	<0.0001	
AD	521.23	1	521.23	72.99	<0.0001	
AE	9.43	1	9.43	1.32	0.2629	
BC	49.98	1	49.98	7.00	0.0148	
BD	212.80	1	212.80	29.80	<0.0001	
BE	60.07	1	60.07	8.41	0.0083	
CD	132.80	1	132.80	18.59	0.0003	
CE	17.03	1	17.03	2.38	0.1368	
DE	133.28	1	133.28	18.66	0.0003	
A^2	2585.85	1	2585.85	362.08	<0.0001	
B^2	748.26	1	748.26	104.77	<0.0001	
C^2	4647.83	1	4647.83	650.81	<0.0001	
D^2	3236.97	1	3236.97	453.26	<0.0001	
E^2	587.10	1	587.10	82.21	<0.0001	
Residual	157.12	22	7.14			
Lack of Fit	153.47	20	7.67	4.22	0.2090	not significant
Pure Error	3.64	2	1.82			
Cor Total	13,309.49	42				
Std. Dev.	2.67		R^2	0.9882		
Mean	40.46		Adjusted R^2	0.9775		
C.V.%	6.61		Predicted R^2	0.9533		
Adequate Precision	36.7178					

The quadratic equation obtained for the relationship between the factors and the lipase immobilization efficiency is shown in Equation (2):

$$Y = 73.91 - 3.72 A - 15.54 B - 1.04 C - 0.89 D + 8.05 E + 6.07 AB - 9.66 AC + 11.42 AD + 1.54 AE + 3.53 BC - 7.29 BD - 3.88 BE - 5.76 CD - 2.06 CE - 5.77 DE - 20.10 A^2 - 10.81 B^2 - 26.95 C^2 - 22.49 D^2 - 9.58 E^2 \quad (2)$$

where Y is immobilization yield, A is the agitation speed (rpm), B is the CRL concentration (g/L), C is the temperature ($^{\circ}$ C), D is the time (hour), and E is the weight of MgO- Al_2O_3 beads (g).

The model also showed a statistically non-significant lack of fit (p -value 0.2090), indicating that the responses are adequate to be employed in this model and the model

satisfactorily fitted to the experimental data. Insignificant lack of fit is very important as a significant lack of fit shows that there might be a contribution in the regressor response relationship that is not accounted for in the model.

There are three factors that show a significant effect towards immobilization efficiency, which are agitation speed, CRL concentration, and weight of beads due to p -value < 0.05 . These parameters show an increment in response value when the value of the parameter increases. After achieving the optimum condition, the immobilization efficiency dropped. The 3D surface plots of immobilization efficiency and the interaction between independent variables are shown in Figure 4. The parameters involved are interaction between agitation speed and temperature (AC), agitation speed and time (AD), and CRL concentration and time (BD), as shown in Figure 4 b, c, f. The 3D response surface in Figure 4(a) reveals that the immobilization efficiency increases by increasing agitation speed (50 to 150 rpm) and CRL concentration (2–4 g/L). However, if a very large quantity of lipase loading (>4 g/L) is introduced, it may reduce the activity recovery, as the enzyme is deposited in the inner pore of $\text{MgO-Al}_2\text{O}_3$, thus, prolonging the contact time of the substrate to reach the enzyme's active site. This result correlates favorably with Rios et al., regarding the increment in the effect of substrate diffusion limitations of p -Nitrophenyl butyrate due to high enzyme loading, subsequently reducing enzyme activity [36]. As reported by Fernandez-Lopez (2017), the enzyme crowding phenomenon, where enzyme stability decreased when enzyme loading increased, caused the activity to drop [37]. Figure 4b shows that with the simultaneous increase in agitation speed and temperature, the immobilization efficiency improved up to a certain optimum value. The non-uniform distribution of the enzyme in the immobilization mixture during the adsorption process can be linked to the low-immobilization yield at 50 rpm of agitation speed [33]. Increasing agitation speed increases immobilization efficiency by providing more adsorption sites [38]. Figure 4c shows that increasing the time and agitation speed ratio from 2 to 4 h and 50 to 110 rpm causes a 20% increment in immobilization efficiency while increasing the weight of the bead between 2 and 2.5 g and agitation speed between 110 and 130 rpm resulted in up to 80% immobilization efficiency, as shown in Figure 4d.

Figure 4e demonstrates that as the incubation temperature rises to 40 °C and the weight of the beads drops, the immobilization efficiency falls. The curvature in Figure 4f shows the interaction between CRL concentration and immobilization time greatly impacts the immobilization efficiency. These results were supported by previous a experiment conducted by Chang et al. [39]. Other interactions shown in Figure 4g portray the interaction between the weight of beads and CRL concentrations. Increased enzyme loading means lots of protein being adsorbed on the support and the increment in weight of beads provides more surface for the enzyme to adsorbed, hence, increasing immobilization efficiency [36]. Figure 4h reveals that there is no significant interaction between immobilization time and temperature, with increasing immobilization time increasing immobilization efficiency, while increasing temperature decreased immobilization efficiency. The results are comparable to research conducted by Andriano Jospin (2017), where the author deduced that the increase in the temperature at a fixed immobilization time induced a reduction in the immobilization yield [40]. In addition, Figure 4i,j portrayed the interaction between the weight of beads and temperature, and also between the weight of beads and incubation time, respectively. These interactions did not represent a significant effect towards immobilization efficiency attributed to p -value > 0.05 . Even though, the immobilization efficiency is still low, the optimization of other independent variables (agitation speed, temperature, time, and weight of $\text{MgO-Al}_2\text{O}_3$ beads) at their optimum value may increase immobilization efficiency after a validation process.

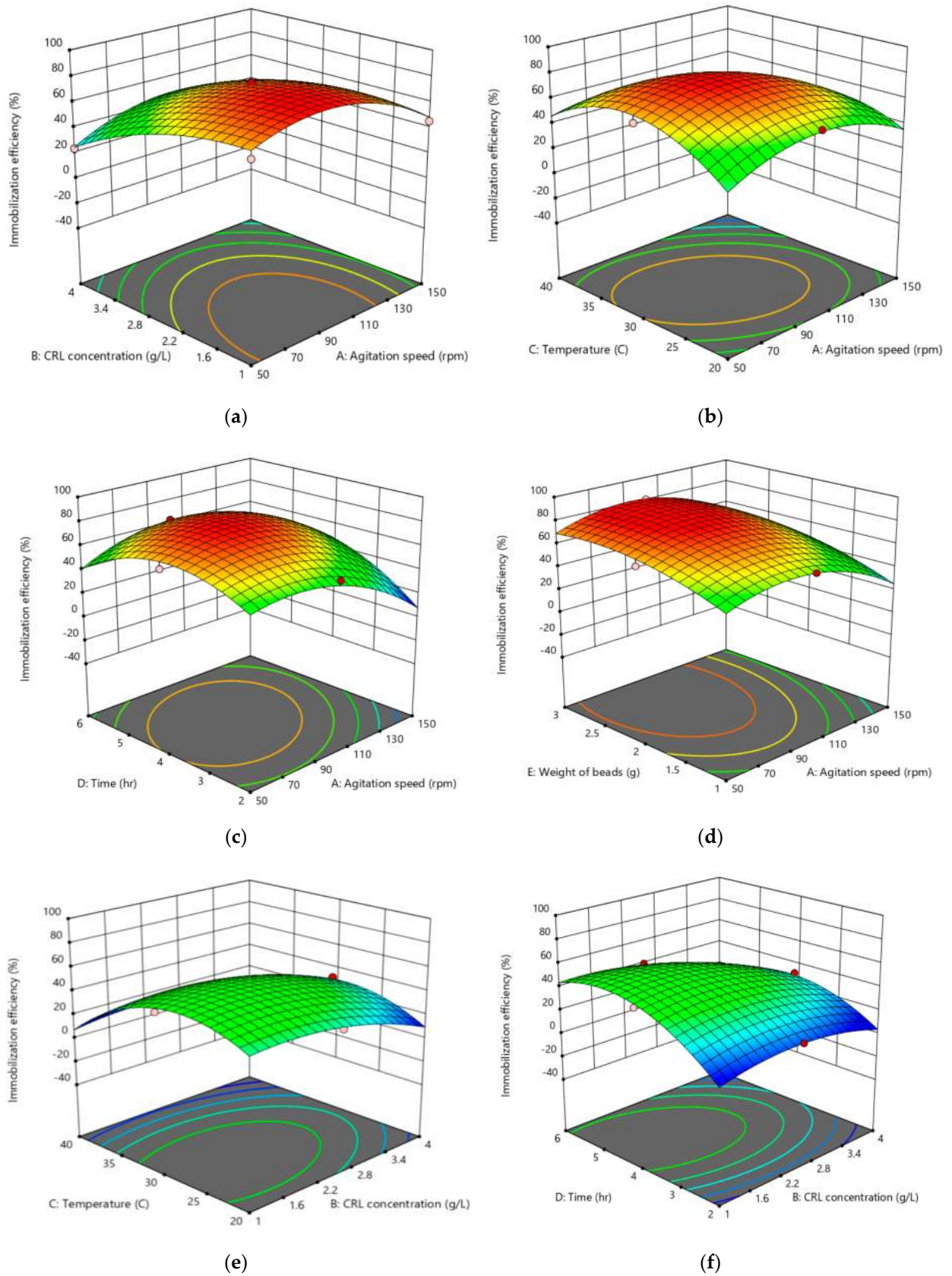


Figure 4. Cont.

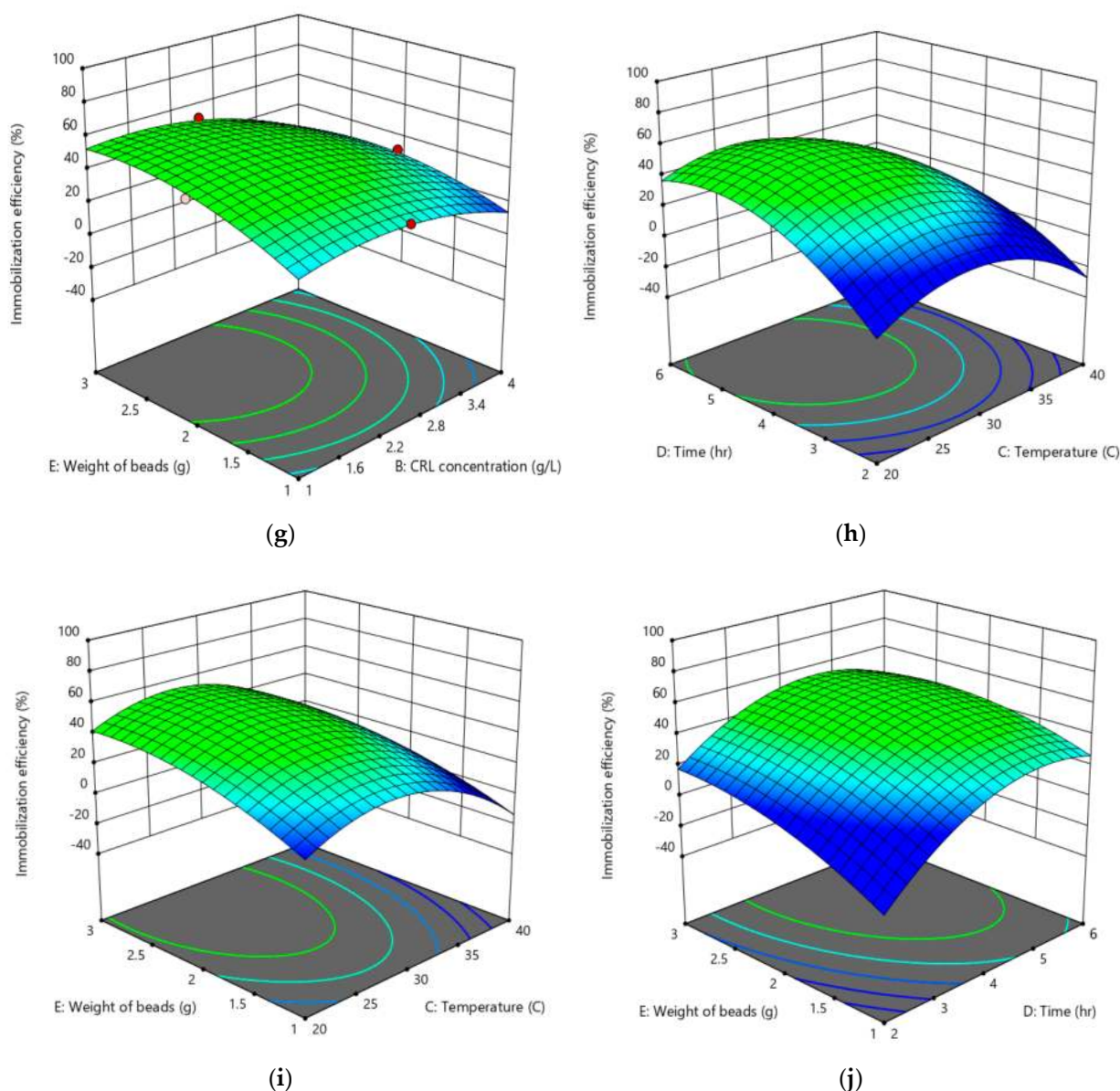


Figure 4. Response surface plot and contour plot for immobilization efficiency showing significant model terms: (a) agitation speed vs. CRL concentration, (b) agitation speed vs. temperature, (c) agitation speed vs. time, (d) agitation speed vs. weight of MgO-Al₂O₃ beads, (e) CRL concentration vs. temperature, (f) CRL concentration vs. time, (g) CRL concentration vs. weight of MgO-Al₂O₃ beads, (h) temperature vs. time, (i) temperature vs. weight of MgO-Al₂O₃ beads, and (j) time vs. weight of MgO-Al₂O₃ beads.

2.5. Validation of the Model

Table 4 shows that the experimental results are quite close to the theoretical calculated data provided by the proposed models. The validation of these parameters (147.2 rpm agitation speed, 3.83 g/L CRL concentration, 20.63 °C temperature, 5.98 h of immobilization time and 2.44 g of MgO-Al₂O₃ beads weight) successfully maximized the activity recovery up to 88.9%. Furthermore, the optimized conditions for activity recovery and immobilization efficiency were obtained as follows: 121.53 rpm agitation speed, 2.84 g/L CRL concentration, 26.96 °C temperature, 4.08 h immobilization time, and 2.69 g of MgO-Al₂O₃ beads (Table 4 (c)). These optimized conditions experimentally resulted in 70.6% of activity recovery and 63.2% of immobilization efficiency. The predicted activity recovery and immobilization efficiency are 71.8% and 65.1%, respectively, and this proves that the experimental

results are relatively close to the computed and projected values by the model. It can also be concluded that the chosen BBD is an accurate and dependable strategy for predicting the response to CRL immobilisation under the conditions tested. The immobilization efficiency and activity recovery of CRL/MgO-Al₂O₃ are comparable to the immobilization of lipase in an octyl-agarose study conducted by Rios et al. [36], resulting in 73.5% and < 75%, respectively. However, the immobilization efficiency and activity recovery in this study are lower than in an immobilization study conducted on mesoporous material MCM-41 [41] and magnesium nano ferrite (MgNF) [42] via covalent bonding, probably due to strong attachment of lipase on the support, preventing leaching of the immobilized enzyme.

Table 4. Results of model validation at the optimum condition for (a) activity recovery and (b) immobilization efficiency (c) activity recovery and immobilization efficiency.

(a) Activity Recovery								
Agitation Speed (rpm)	CRL Concentration (g/L)	Temperature (°C)	Time (Hour)	Weight of MgO-Al ₂ O ₃ Beads (g)	Activity Recovery (%)		Immobilization Efficiency (%)	
					Predicted Value	Experimental Value	Predicted Value	Experimental Value
147.20	3.83	20.63	5.98	2.44	88.9	85.7	16.2	17.9
(b) Immobilization efficiency								
97.96	1.41	28.06	4.13	2.36	53.7	53.5	82.3	80.0
(c) Activity recovery and immobilization efficiency								
121.527	2.845	26.964	4.076	2.690	71.8	70.6	65.1	63.2

2.6. Biochemical Characterization of CRL/MgO-Al₂O₃ and free CRL

2.6.1. Thermal and pH Stability

One of the most significant qualities for practical application, particularly in industry, is the temperature stability of immobilized lipase. The experimental method of biochemical characterization is described in the Supplementary Materials. Figure 5a,b shows the free CRL was retaining its activity better compared to CRL/MgO-Al₂O₃. At 40 °C, both free CRL and CRL/MgO-Al₂O₃ show no significant loss in lipase activity. However, when temperature increases to 50 °C, the residual activity for CRL/MgO-Al₂O₃ after 75 min incubation dropped to 54.7% of its initial activity, while the residual activity free CRL was observed at 75.9%. A further increment in temperature (60 and 70 °C) led to a declination in residual activity for both free CRL and CRL/MgO-Al₂O₃. After 75 min incubation at 60 °C and 70 °C, the residual activity for free CRL declined to 64.2% and 47.3%, respectively, which is higher compared to the residual activity of CRL/MgO-Al₂O₃ with 32.7% and 22.7%, respectively. This result displayed contradictions with the earlier findings by Wenlei Xie et al., in which the immobilized CRL on a graphene oxide sheet exhibited better thermal stability compared to free CRL [43]. The possible reasons for the reduction in residual activity of CRL/MgO-Al₂O₃ at high temperatures are due to thermal energy diffusivity from the Al₂O₃ wall (thermal conductivity of Al₂O₃ 30–40 W/mK) [44] and enzyme structural changes at β-sheet after heat treatment [34].

Furthermore, the pH stability for free CRL and CRL/MgO-Al₂O₃ was determined by incubation at different pH ranges from 4 to 10. Figure 5c shows that almost 50% of activity recovery was obtained by CRL/MgO-Al₂O₃. In addition, at pH 4–8, free CRL exhibited superior pH stability compared to CRL/MgO-Al₂O₃. Immobilization may affect the structural stability of enzymes because of the changes in the total net charges of the enzymes caused by the ionization of acidic and basic amino acid side chains in the microenvironment around the active site of the enzyme [45,46]. In addition, in an extreme alkaline environment (pH 10), the stability of free CRL drastically decreased as compared to CRL/MgO-Al₂O₃ due to a break down of hydrogen bonds in water–protein interactions in an extreme pH microenvironment.

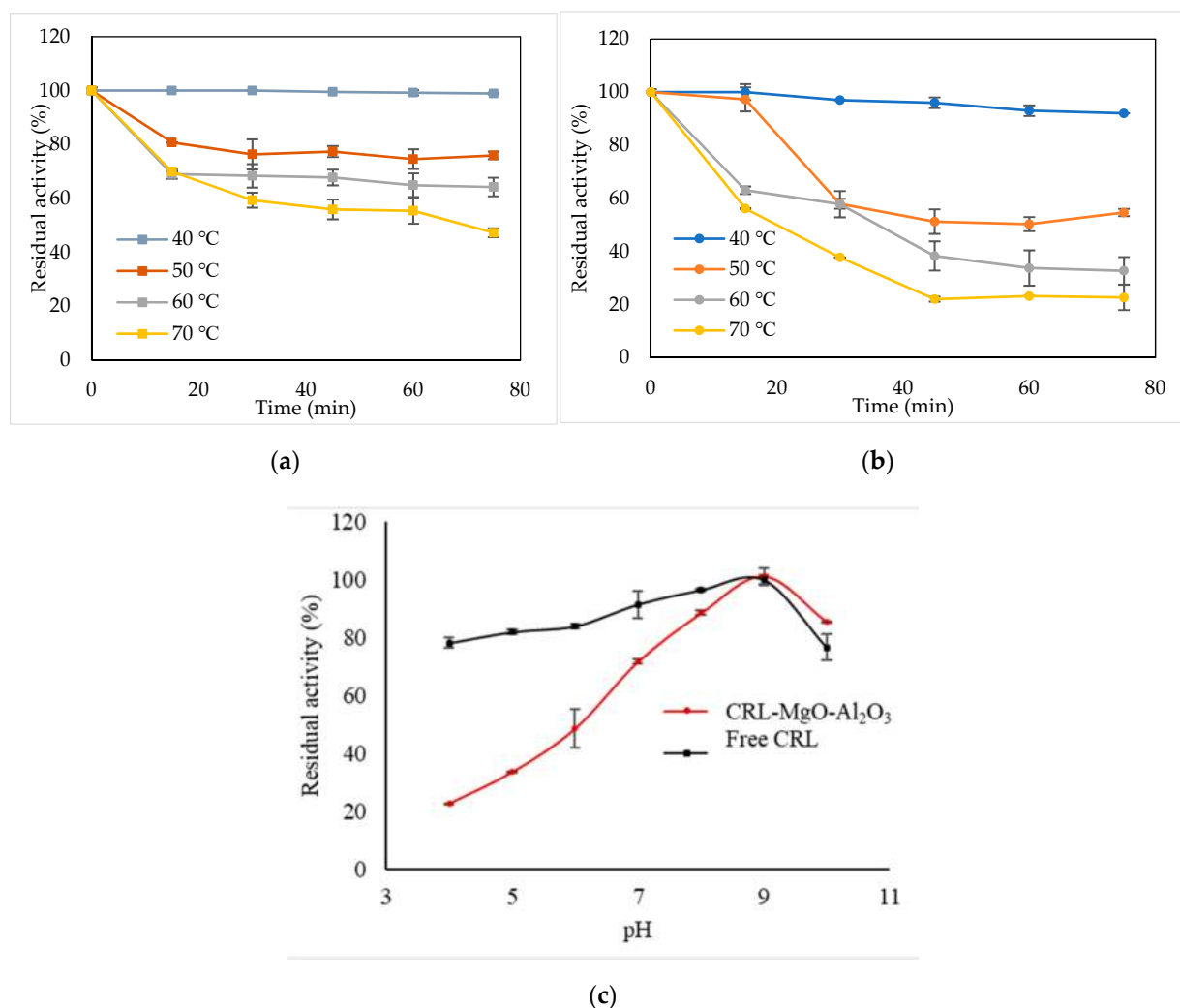
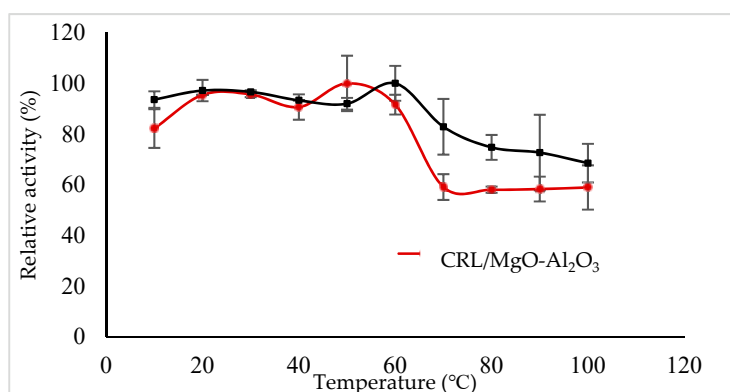


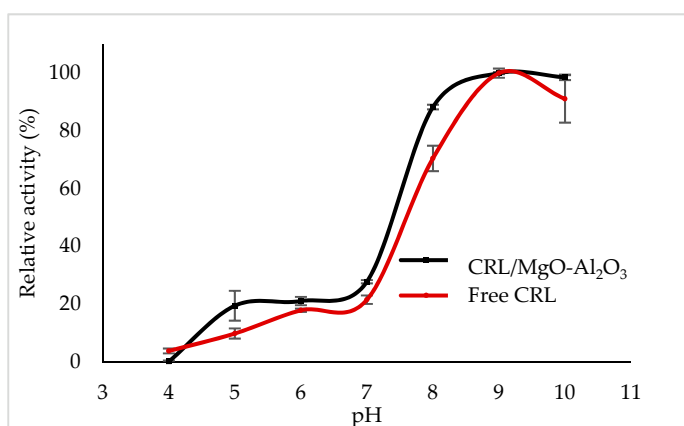
Figure 5. Thermal stability of (a) free CRL and (b) CRL/MgO-Al₂O₃ at 40, 50, 60, and 70 °C while (c) pH stability for free CRL and CRL/MgO-Al₂O₃. The initial activity of free CRL and CRL/MgO-Al₂O₃ before being incubated at varying ranges of temperature and pH was set as 100%. The error bars show standard deviations; all studies were conducted in triplicate.

2.6.2. Optimum Temperature and pH

The effect of temperature on the relative activities of free CRL and CRL/MgO-Al₂O₃ was studied by measuring the enzyme activity at a particular temperature in a range of 10 °C to 80 °C (Figure 6a). The optimum temperature for CRL/MgO-Al₂O₃ dropped to 50 °C, lower than that of free CRL (60 °C), as shown in Figure 6a. The shift in optimum temperature of CRL could be described by the formation of hydrogen bonds between enzyme molecules with support during immobilization, which could lead to three-dimensional structural changes in the enzyme [47]. The influence of pH on the relative activity of the free CRL and CRL/MgO-Al₂O₃ was determined in a range of pH 4–10. The results in Figure 6b demonstrated that free CRL and CRL/MgO-Al₂O₃ have the same optimum pH of 9. It reveals that the immobilization method did not affect CRL's optimal pH.



(a)



(b)

Figure 6. (a) Optimum temperature of free CRL and CRL/MgO-Al₂O₃ at 60 and 50 °C, respectively while (b) pH optimum for free CRL and CRL/MgO-Al₂O₃ at pH 9. The highest activity of free CRL and CRL/MgO-Al₂O₃ was defined as 100% of relative activity. The error bars show standard deviations; all studies were conducted in triplicate.

2.6.3. Mechanical Stability, Leaching Analysis, and Reusability

To further examine the stability of CRL/MgO-Al₂O₃, mechanical stability and leaching analyses were conducted. Figure 7 illustrated that, at lower agitation speeds (50 and 100 rpm), CRL/MgO-Al₂O₃ retained 97.7% and 72.4% of their initial activity with a lower enzyme leaching percentage of 13.99% and 10.96%, respectively. At 150, 200, and 250 rpm of agitation speed, the residual activity of CRL/MgO-Al₂O₃ reduced to 69.0%, 65.1%, and 61.8%, respectively. In general, when operating at 50 to 250 rpm for 60 min, the enzyme leaching out from the support was less than 14%, which is comparable to a previous study conducted by George et al., where 15% of lipase leached out from the support [48]. Even though the study employed covalent bonding through interaction between lipase and silanol groups of mesoporous silica, the percentage of enzyme leached is slightly higher than in our study, suggesting that physical adsorption is suitable for industrial application, especially in non-aqueous media [49]. Enzyme leaching is mainly due to the physical attachment of the enzyme on the support via Van der Waals forces and hydrogen bonding [50].

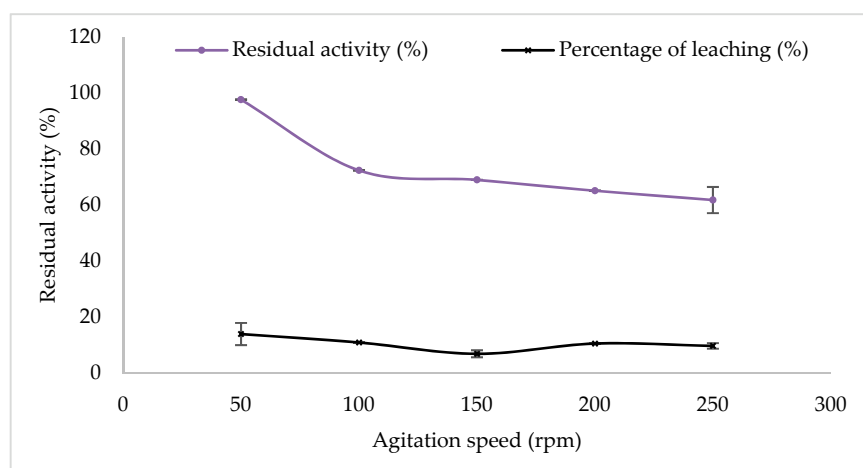


Figure 7. The residual activities of CRL/MgO-Al₂O₃ after shaking at various agitation speeds for 60 min at 30 °C. The initial activity of CRL/MgO-Al₂O₃ before being incubated at various ranges of agitation speed was set as 100%. The error bars represent the standard deviation of triplicate experiments.

Figure 8 shows the reusability of CRL/MgO-Al₂O₃ on the residual activity of the *p*-NPP hydrolysis. CRL/MgO-Al₂O₃ preserved more than 32.7 percent of its initial activity after 12 cycles. Up to nine cycles, CRL/MgO-Al₂O₃ is able to retain 50% of its initial residual activity. The decrease in activity recovery of CRL/MgO-Al₂O₃ after 12 cycles was most likely due to the washing during separation steps that induced enzyme leaching or desorption of non-covalently bound enzyme molecules from the support [51]. The immobilization of CRL on MgO-Al₂O₃ by adsorption shows 72.9% residual activity after 5 cycles, which is higher when compared to immobilized *Candida Antartica* (isoform B lipase) on octyl agarose and coated with the polymers (polyethyleneimine and dextran) with ~65% residual activity [52]. Even though the addition of polymers reduced the percentage of enzyme leaching during thermal inactivation and improved enzyme stability, the enzyme recyclability in our study is superior. CRL/MgO-Al₂O₃ shows better recyclability compared to *Candida Antartica* lipase immobilized on acrylic resin synthesized by Amini et al. that showed recyclability up to only 10 cycles, with a 21.5% product yield [53]. In addition, our reusability study is 1.64-fold higher compared to the immobilized CRL on modified polyethersulfone, which yields only 20% of residual activity after 12 consecutive cycles [54]. The decrease in CRL activity in future cycles could be due to a variety of factors, including enzyme denaturation, enzyme leaching from the support, and aggregation of reaction products on the support and enzyme, all of which limit the accessibility of the substrate to the enzymes' active sites [50].

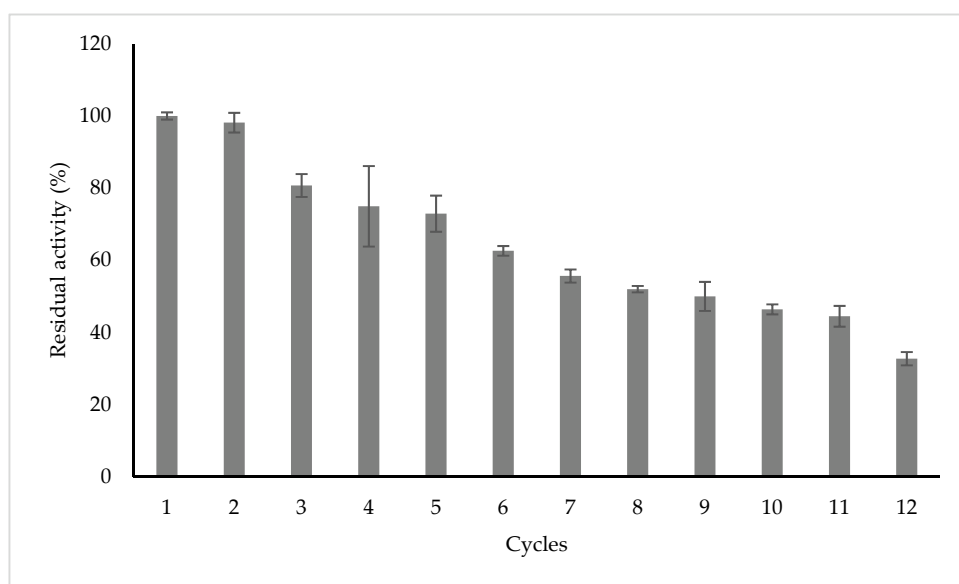


Figure 8. Reusability of CRL/MgO-Al₂O₃ for 12 cycles. All experiments were performed in triplicate; the error bars represent standard deviations. The first cycle of CRL/MgO-Al₂O₃ for lipase assay was set as 100%.

2.6.4. Solvent Tolerance Analysis

The stability of lipases in the presence of solvents is crucial, especially in the reaction that involved esterification and transesterification to make biodiesel. One of the major drawbacks adopting an enzymatic catalyst in biodiesel production is the low tolerance of lipases towards the acyl acceptor. One of the methods to reduce the negative effect of the alcohol on the enzyme is the addition of organic solvents. Free CRL and CRL immobilized onto MgO-Al₂O₃ were incubated in the presence of solvents with different concentrations for 30 min. Figure 9a shows that the residual activity of free CRL decreased as the concentration of solvents increased. At 5% (*v/v*) concentration of solvents, free CRL does not show a significant reduction in relative activity when compared to lipase without solvent addition, except for methanol. The residual activity for free CRL was 100.55%, 91.45%, and 100.13% after being incubated at 5% (*v/v*) concentration of ethanol, isopropanol, and tert-butanol for 30 min. The residual activity after being incubated at 5% (*v/v*) methanol resulted in 72.46% and the relative activity increased to 81.05% at 20% (*v/v*) of methanol concentration and decreased afterwards. The residual activity of free CRL after incubation at 50% (*v/v*) concentration of ethanol, methanol, and tert-butanol for 30 min was 39.03%, 55.25%, and 23.81, respectively. The hydrophobic interactions, hydrogen bonds, and electrostatic interactions of protein can be affected by solvents by changing their conformational structure. Solvents with high polarity, such as methanol and ethanol, cause a conformational change in native form to inactive form by partial removal of water from the catalytic site of the enzyme, reducing its catalytic efficiency [55]. Incubation in 5% to 20% (*v/v*) concentration of tert-butanol showed the lipase is able to retain its catalytic activity up to 97.60% and declined to 46.91% after being incubated in 30% of tert-butanol. Free lipase can tolerate tert-butanol more readily because of the retention of a water layer that hydrates the enzyme and prevents it from unfolding. Compared to solvents with linear structures, tert-butanol has branching structures that increase the stability of enzyme activity and conformation [55].

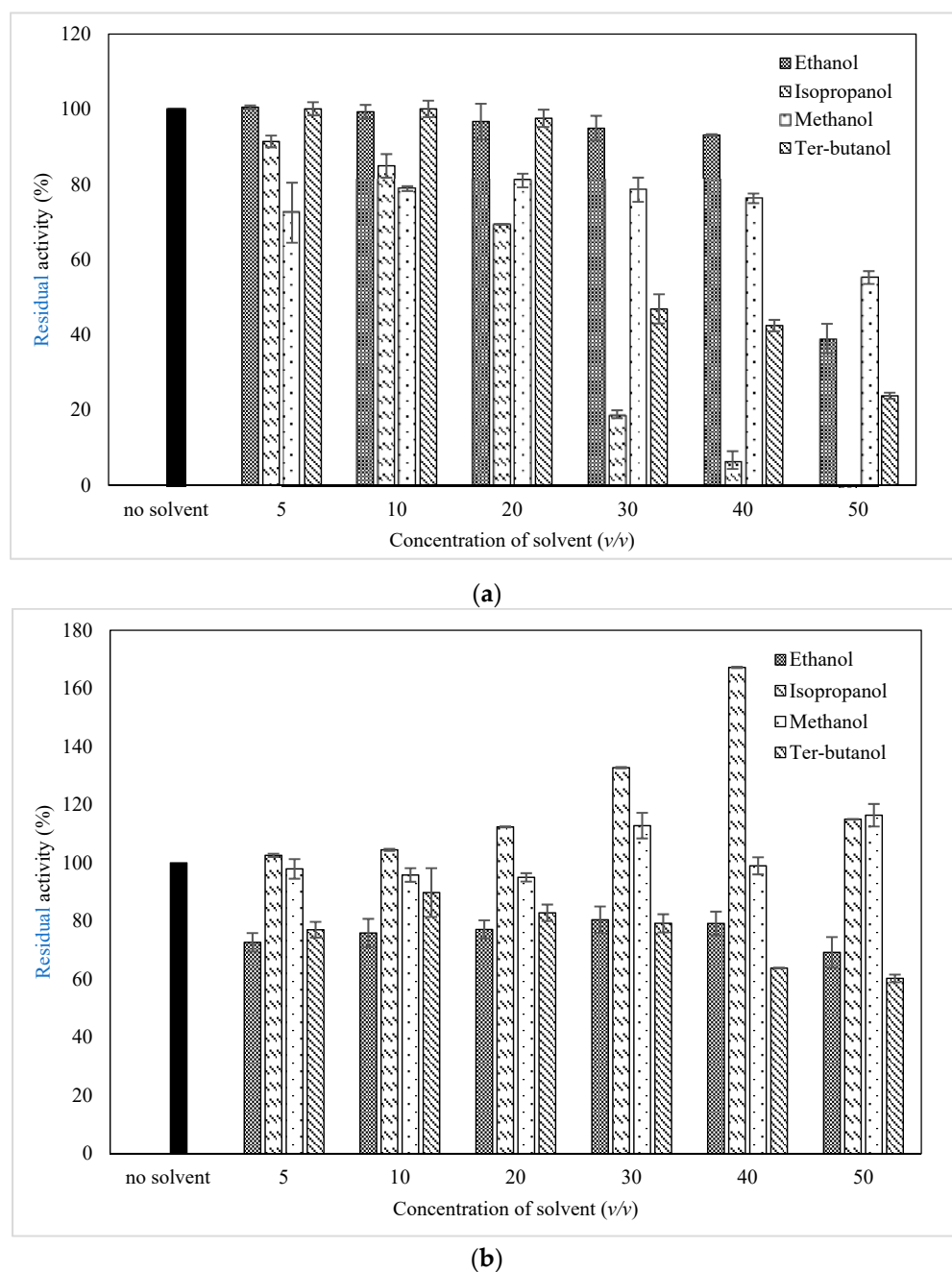


Figure 9. Solvent tolerance analysis of (a) free CRL and (b) CRL/MgO-Al₂O₃ at 5, 10, 20, 30, 40, and 50% (v/v) of solvent concentration. The 100% of residual activity for CRL and CRL/MgO-Al₂O₃ indicated as the initial lipase activity without solvent addition.

Figure 9b depicted that among four types of solvents (ethanol, isopropanol, methanol, and tert-butanol) that were evaluated, isopropanol was the most tolerant in terms of immobilized lipase stability. In general, compared to free CRL, CRL/MgO-Al₂O₃ showed an increment in residual activity in 50% (v/v) concentration of ethanol, isopropanol, methanol, and tert-butanol correspond to 69.18, 114.99, 116.37, and 60.24%, respectively. Immobilization of CRL on MgO-Al₂O₃ improves the inner rigidity of the lipase structure, preventing the water at the protein interface from being stripped off, eventually retaining the catalytic conformation of lipase [56]. These findings demonstrated that the denaturing effects of solvents can be reduced because the enzyme structure is stable due to its fixation to the support, hence, minimizing activity loss. This study corresponds with the reports

published by Badoei-Dalfard et al. [57] and Ingrid Y. Pulido et al. [58], in which the immobilized lipase presented higher residual activity after being incubated in 50% and 30% (*v/v*) concentration of solvents (methanol, ethanol), respectively, compared to free lipase. CRL/MgO-Al₂O₃ presented hyperactivation after incubation from 5% to 40% (*v/v*) of isopropanol increased with 102.61% and 167.21% of residual activity, respectively. After incubation in 50% (*v/v*) of isopropanol, the relative activity of CRL/MgO-Al₂O₃ dropped drastically to 114.99%, but portrayed hyperactivation when compared to the initial activity of immobilized CRL and free CRL. On the contrary, for free CRL, a complete loss of lipase activity was observed after incubation in 50% (*v/v*) of isopropanol. Due to the hydrophobic nature of the lipase's active site, the hydrophobic region on the isopropanol may bind to the active site, induce perturbation, and alter the catalytic triad of the enzyme [59,60]. The resistance of CRL/MgO-Al₂O₃ towards different types of solvent could expand its potential for various applications, especially in biofuel synthesis. Alcohols have been used widely as an acyl acceptor in biodiesel production. However, deactivation of lipases may occur at high alcohol-to-oil molar ratios; thus, a stepwise addition of alcohol was implemented to minimize lipase deactivation [61]. Moreover, the addition of co-solvents may reduce the inhibitory effect of alcohols towards lipases by controlling the concentration of alcohols surrounding the lipases [62] and enhance the solubility of the substrate [63]. These methods are laborious and lead to additional costs and environmental concerns [63]. The prepared CRL/MgO-Al₂O₃ shows high stability of lipase in four types of alcohol that are commonly used in biodiesel production, thus, eliminating the addition of solvents in the reaction system.

2.7. Physical Characterization of CRL/MgO-Al₂O₃

The study of the surface chemistry of the support materials is important to gain a better understanding of the chemical and physical processes that happen between enzymes and the surface of the support. The elemental analysis of the prepared Mg by ICP-OES showed that the concentration of Mg in the prepared support was 0.96 mg/L, which is higher than the Mg content in the native Al₂O₃ with 0.10 mg/L (as shown in Table 5). The native Al₂O₃ contains impurities, such as metal precursors (Mg, Ca, Si and Fe), that interfere during the manufacturing process. Our findings appear to be well supported by Romero Toledo et al., who discovered 0.9 wt.% of Mg was quantified in Al₂O₃ [13]. The Mg content in the CRL/MgO-Al₂O₃ increased due to the presence of trace metal in the phosphate buffer that was used to dissolve the enzyme.

Table 5. ICP-OES analysis for Mg detection on different samples.

Sample	Concentration of Mg (mg/L)
Al ₂ O ₃	0.10
MgO-Al ₂ O ₃	0.96
CRL/MgO-Al ₂ O ₃	1.05

The TGA-DTA spectra curves for the dried Al₂O₃, MgO-Al₂O₃, and CRL/MgO-Al₂O₃ are represented in Figure 10. This analysis was employed to observe the decomposition and degradation of the catalysts by measuring the changes in samples' weight over time as the temperature changes and its thermal stability at high temperature [64]. The first stage of decomposition for Al₂O₃ and MgO-Al₂O₃, attributed to the desorption of moisture content, occurred in a temperature range of 45 °C to 140 °C and 45 °C to 150 °C, corresponding to 5% and 9% of weight loss, respectively [65]. Next, the second stage of decomposition of Al₂O₃ occurred at 140 °C to 660 °C, accompanied by a weight loss of 8%, attributed to the decomposition of boehmite and the formation of γ -Al₂O₃ aluminum oxide [15]. The precise temperature for the transformation of distinct Al₂O₃ phases (γ -Al₂O₃, δ -Al₂O₃, θ -Al₂O₃, α -Al₂O₃) can be determined via continuous measurement during thermal analysis. Meanwhile, the decomposition of nitrate in MgO-Al₂O₃ occurs at the second stage, resulting in a % of weight loss occurring at 150 °C to 650 °C, since all of the catalysts were prepared

with nitrate precursors [66]. At the last stage of $\text{MgO-Al}_2\text{O}_3$ thermal degradation, no formation of volatile gases was detected, forming pure magnesium oxide [64]. The results show that the formation of pure $\text{MgO-Al}_2\text{O}_3$ can be obtained through calcination at $800\text{ }^\circ\text{C}$, evidenced by the constant weight of the catalyst. However, the best calcination temperature used for this CRL immobilization was $300\text{ }^\circ\text{C}$, indicating that the CRL favors immobilization on a magnesium precursor instead of pure magnesium oxide.

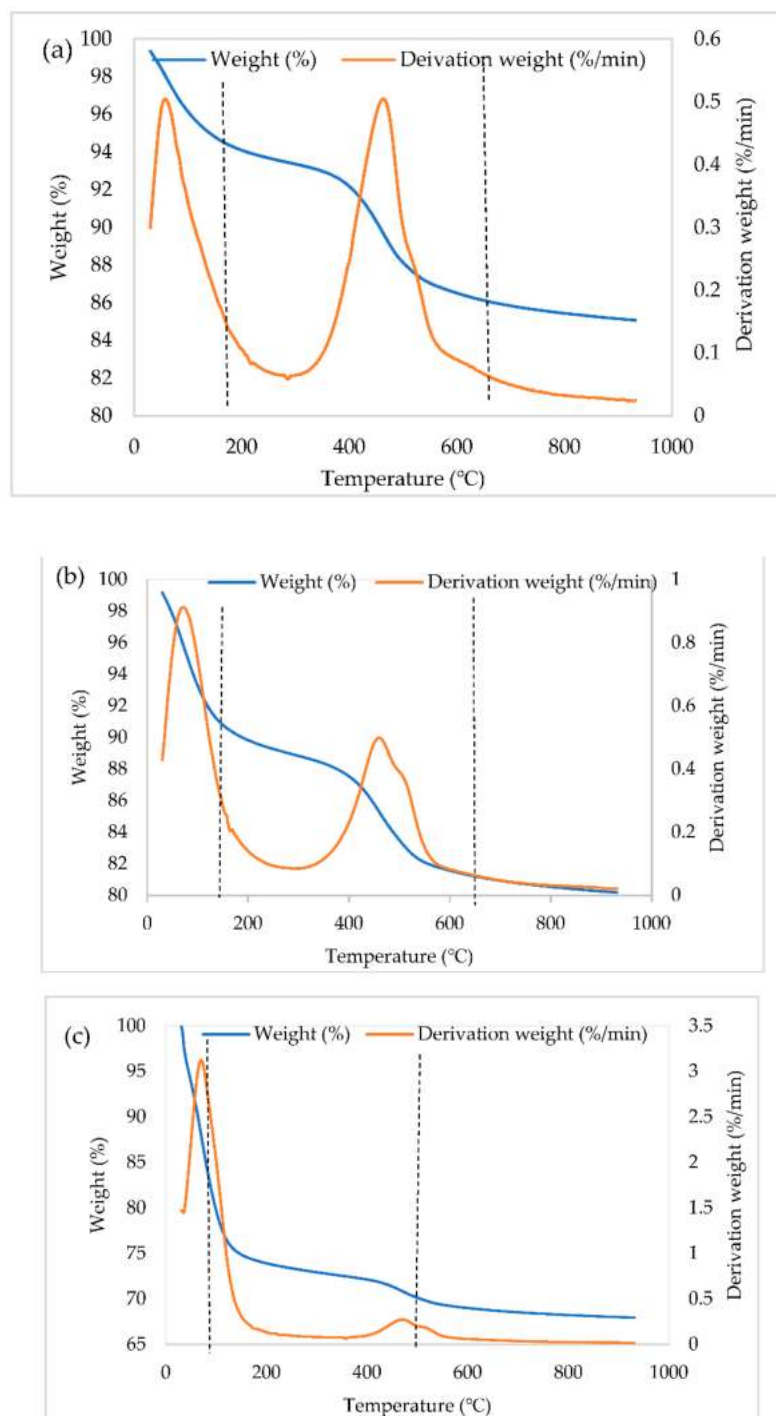


Figure 10. TGA-DTA spectra of the (a) support (Al_2O_3), (b) adsorbed metal oxide ($\text{MgO-Al}_2\text{O}_3$) species taken after heating at $300\text{ }^\circ\text{C}$, and (c) CRL immobilized on the support ($\text{CRL/MgO-Al}_2\text{O}_3$).

The thermal analysis revealed that the composition of organic matter was increased after CRL immobilization on MgO-Al₂O₃, resulting in greater weight loss of CRL/MgO-Al₂O₃ compared to MgO-Al₂O₃ and Al₂O₃. The first stage of decomposition of CRL/MgO-Al₂O₃ can be observed at temperatures ranging from 45 to 160 °C, resulting in a 25% major loss of weight due to decomposition of immobilized lipase [67]. The enzyme loading on CRL/MgO-Al₂O₃ was calculated to be 14.26% based on the comparison of TGA curves of CRL/MgO-Al₂O₃ and MgO-Al₂O₃. This finding was supported by a previous study conducted by Patel et al., where at roughly 100 °C, the immobilization of CRL on ZnO revealed a 10% weight loss, which is attributed to the loss of water molecules and thermal decomposition of lipase, showing effective enzyme immobilization on the platform [68]. It has been suggested that apart from the material properties of metal oxides, types of enzymes and buffers also have significant effects on the adsorption strength during the immobilization process [20].

The FTIR spectra of magnesium oxide impregnated on Al₂O₃ and CRL immobilized on MgO-Al₂O₃ catalysts are shown in Figure 11. The observation of the effect of MgO towards the adsorption of the enzyme was analyzed using FTIR. The purpose of this analysis is to characterize the surface-adsorbed species over binary oxide and catalysts. The valley between 1069 cm⁻¹ and 482 cm⁻¹ of Al₂O₃ confirms the γ -form and the one at 723 cm⁻¹ is assigned to the bending vibrations of the Al-O-Al bond [69]. The peaks in the region of 500–750 cm⁻¹ are assigned to Al-O, whereas the shoulder at 750 and the line at 890 cm⁻¹ are assigned to Al-OH species. Thus, the γ -Al₂O₃ phase contains both tetrahedral and octahedral coordination [15]. The peaks at 723 cm⁻¹, 588 cm⁻¹, and 495 cm⁻¹ correspond to twisting, stretching, and bending vibrations between the aluminium and oxide [70].

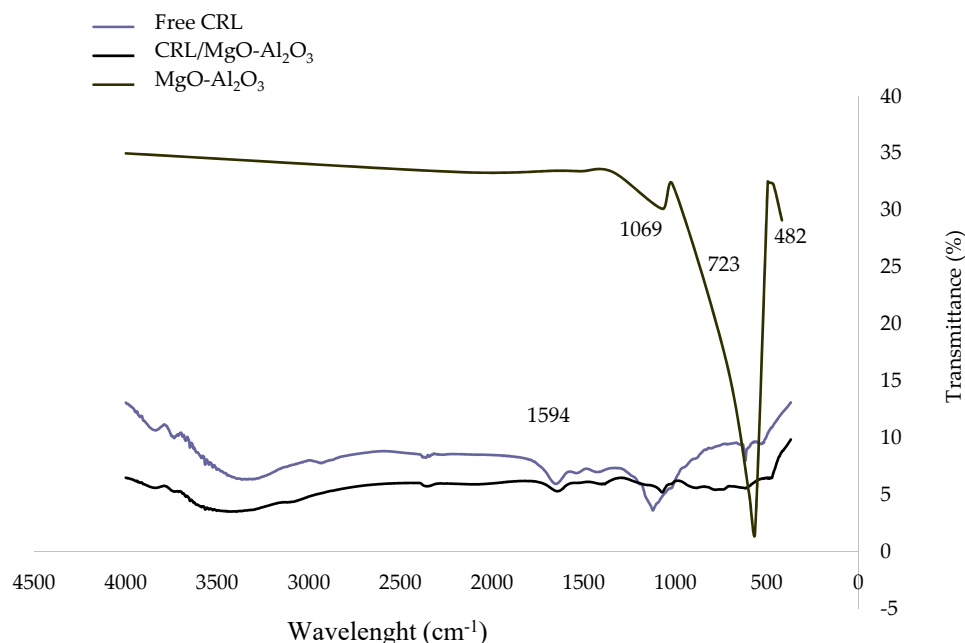


Figure 11. Fourier transform infrared spectra of the support (Al₂O₃), adsorbed metal oxide (MgO-Al₂O₃) species taken after heating at 300 °C, and CRL immobilized on the support (CRL/MgO-Al₂O₃).

The FTIR results show a low percentage of surface OH groups for Al₂O₃, indicating a lower acidity due to the low concentration of Al-OH species [13]. For all samples, the wavelength ~1100 cm⁻¹ C-O bond of secondary alcohol was presently attributed to the presence of an alcohol precursor during the production of aluminium oxide. The reaction between metallic aluminium with isopropyl, sec-butyl, or other alcohols takes place to form aluminium alkoxide, the starting materials for the production of aluminium oxide [71]. Specifically, the FTIR peak for MgO-Al₂O₃ was the same as Al₂O₃ due to a redundant MgO peak at 836 cm⁻¹ with the peak of Al₂O₃. However, the presence of Mg into the

Al crystal lattice changed the acid and basic properties of this oxide [69]. The presence of magnesium decreases the Brønsted acidity and increases the basicity of alumina due to the lower electronegativity of magnesium (1.31) compared to aluminium (1.61) [69]. All of the samples show a small peak at 1649 cm^{-1} , corresponding to the bending–scissoring vibrations (H-O-H) of water molecules due to the physisorbed water.

The –OH bending vibration can be observed at 1069 cm^{-1} , due to the in-plane bending–scissoring vibration of OH in Al–O–H [15]. After lipase immobilization, the characteristic peak appearing at 1594 cm^{-1} could be attributed to C=O stretching (amide I band) and N–H bending vibrations (amide II band) from amide (–CO–NH–), respectively [72]. The enzyme’s protein backbone is responsible for the related peaks of amide-type I and amide-type II [73]. The successful immobilization of CRL on the support was confirmed by the broadening and increasing intensity of the characteristic absorption peaks of CRL in the FTIR spectrum of CRL/MgO–Al₂O₃.

Figure 12 illustrated the FESEM image of Al₂O₃, MgO–Al₂O₃, and CRL/MgO–Al₂O₃. This analysis was used to observe the morphology of the support and confirm the deposition of CRL on the support. Rough surface morphology with a combination of larger and smaller particle sizes and the formation of aggregates and agglomerates with undefined shapes can be observed on the pure Al₂O₃ pellet (Figure 12a,b). Figure 12c,d show that the catalyst surfaces impregnated with a magnesium precursor were scattered and densely packed with coarse and non-uniform grain structures, resembling disc-shaped morphology. The sintering effect on the MgO–Al₂O₃ formed a larger particle size and showed a good bonding structure with a smooth stacking particle indicating a good diffusion process, as compared to the pure Al₂O₃ pellet. Moreover, Figure 12c,d depicted that the surface of Al₂O₃ was covered with the magnesium precursor and the results were supported with TGA analysis, confirming that the calcination of the catalyst at $300\text{ }^{\circ}\text{C}$ was not enough to form pure magnesium oxide. Previous work by Harun et al. showed that MgO can stabilize the microstructure of Al₂O₃ by suppressing the grain growth distribution and allowing the porous region to densify homogeneously, without the occurrence of abnormal grain growth [74]. After CRL immobilization, the appearance of a spherical aggregate on the surface of MgO–Al₂O₃ confirmed the immobilization of lipase clusters by physical adsorption (Figure 12e,f). The observations were supported by previous findings by Mohammadi et al. confirming the lipase adsorption by its good dispersion on the carrier.

The characterization of the porous catalysts was performed by measuring nitrogen an adsorption–desorption isotherm. The analysis of BET surface area (Table 6) shows that the impregnation of MgO on Al₂O₃ and immobilization of CRL on MgO–Al₂O₃ led to an increment and decrement in surface area of $301.44\text{ m}^2/\text{g}$ and $246.88\text{ m}^2/\text{g}$, respectively. This study shows similar results to a study conducted by Nematian et al. [73] in regards to the employment of graphene oxide with Fe₃O₄, showing an increment in surface area. These findings suggest that MgO can speed up and increase densification during the sintering stage, resulting in a reduction in the consolidated structure’s porosity value [74]. The pore volumes of Al₂O₃, MgO–Al₂O₃, and CRL/MgO–Al₂O₃ were measured using single-point adsorption. The result shows a decrement in pore volume, attributed to the impregnation of MgO and CRL immobilization with $0.40\text{ cm}^3/\text{g}$, $0.41\text{ cm}^3/\text{g}$, and $0.381\text{ cm}^3/\text{g}$ of Al₂O₃, MgO–Al₂O₃, and CRL/MgO–Al₂O₃, respectively. In contrast, the pore size of Al₂O₃ and MgO–Al₂O₃ decreases after impregnation of MgO and CRL immobilization, respectively.

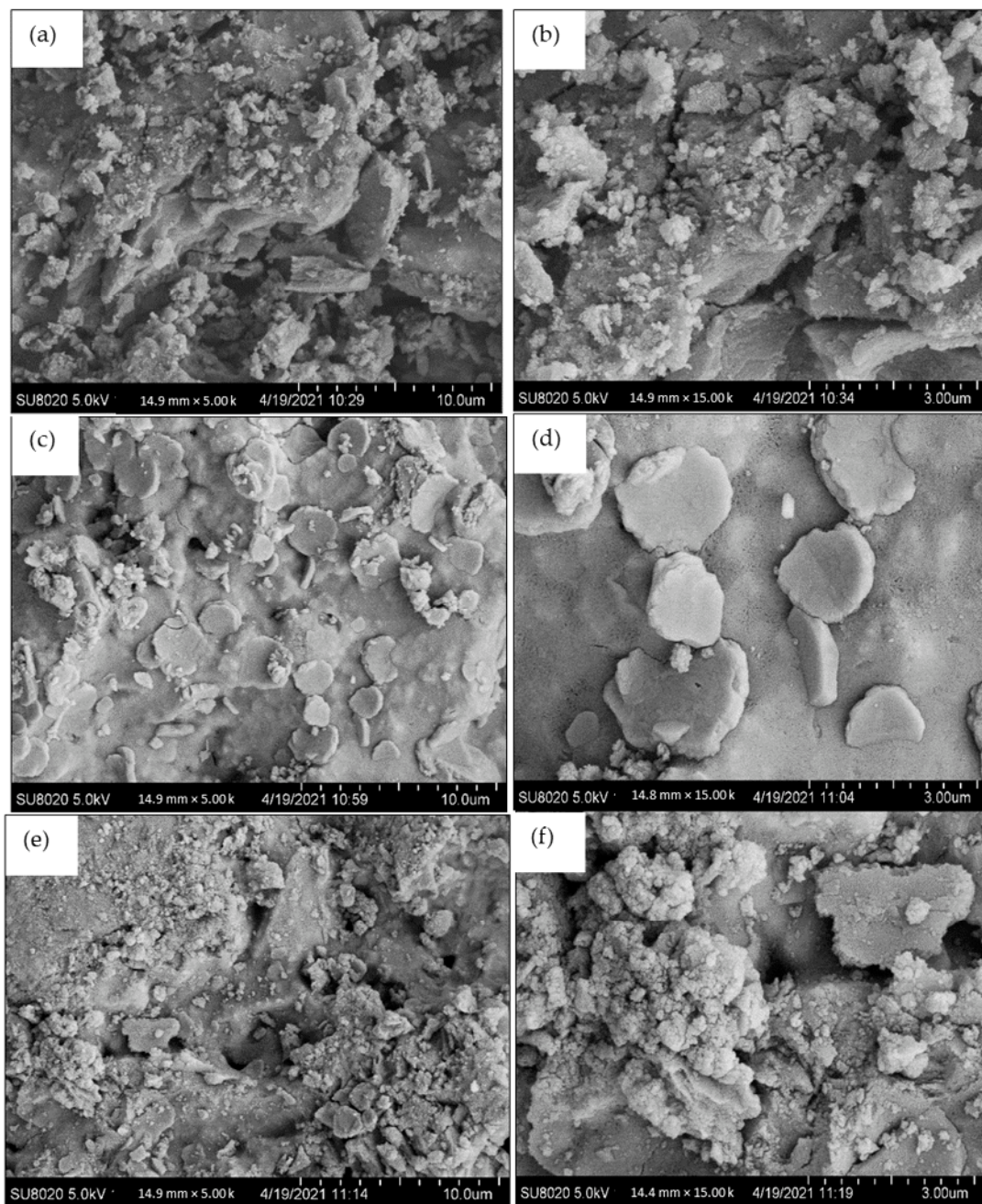


Figure 12. FESEM micrograph of Al_2O_3 , $\text{MgO-Al}_2\text{O}_3$, and $\text{CRL/MgO-Al}_2\text{O}_3$ with magnification $5000\times$ (a,c,e) and $15,000\times$ (b,d,f) magnification, respectively.

Table 6. BET surface area, total pore volume, and pore size evaluated by nitrogen adsorption-desorption and isoelectric point (IEP) of the support and immobilized CRL.

Sample	BET Surface Area (m^2/g)	Total Pore Volume (cm^3/g)	Pore Size BJH (\AA)	IEP
Al_2O_3	275.69	0.40	60.53	3.71
$\text{MgO-Al}_2\text{O}_3$	301.44	0.41	57.13	8.10
$\text{CRL/MgO-Al}_2\text{O}_3$	246.88	0.38	61.53	NA

In order to understand the influence of MgO loading on the surface of the Al_2O_3 , as well as the effect of CRL immobilization on $\text{MgO-Al}_2\text{O}_3$, the nitrogen adsorption-

desorption isotherms were measured. In addition, porous solid materials are classified by the adsorption–desorption isotherm, addressing the relationship between pore size and sorption ability. As illustrated in Figure 13, Al_2O_3 , $\text{MgO-Al}_2\text{O}_3$, and $\text{CRL/MgO-Al}_2\text{O}_3$ were classified according to IUPAC as mesoporous structures because the adsorption–desorption isotherm displays a type IV isotherm, accompanied with hysteresis loop type 3 [75]. The hysteresis loops in the relative pressure for Al_2O_3 , $\text{MgO-Al}_2\text{O}_3$, and $\text{CRL/MgO-Al}_2\text{O}_3$ are similar, which is $P/P_0 = 0.45\text{--}1$, which explains the degree of mesoporosity does not change by the impregnation of MgO on the Al_2O_3 and immobilization of CRL on $\text{MgO-Al}_2\text{O}_3$. Our findings show a good agreement with Mahlambi et al. regarding $\gamma\text{-Al}_2\text{O}_3$, carbon-covered $\gamma\text{-Al}_2\text{O}_3$ and impregnation of TiO_2 on carbon-covered $\gamma\text{-Al}_2\text{O}_3$ exhibited type IV isotherm with heterogeneous pore structure [76]. The N_2 as an adsorbate fills in the mesopore structure at a small pressure and as the concentration of N_2 increases, the formation of a multimolecular adsorption layer occurs when the N_2 fills in the pores of larger diameter. Referring to pore sizes, average pore diameter of Al_2O_3 , $\text{MgO-Al}_2\text{O}_3$, and $\text{CRL/MgO-Al}_2\text{O}_3$ was characterized as macroporous materials ($>50 \text{ \AA}$), corresponding to 60.53 \AA , 57.1 \AA , and 61.533 \AA , respectively [75]. These findings show that the Al_2O_3 , $\text{MgO-Al}_2\text{O}_3$, and $\text{CRL/MgO-Al}_2\text{O}_3$ consist of a distinct mesopore and macropore regime, confirming the existence of the bimodal nature of the pore system in the respective materials. This study concurs well with a porosity analysis of $\text{Ni/Al}_2\text{O}_3$ that showed the bimodal nature in the pore system, with 2/3 of the total pore volume of $\text{Ni/Al}_2\text{O}_3$ having macropores and the remaining 1/3 was a mesopore structure [77].

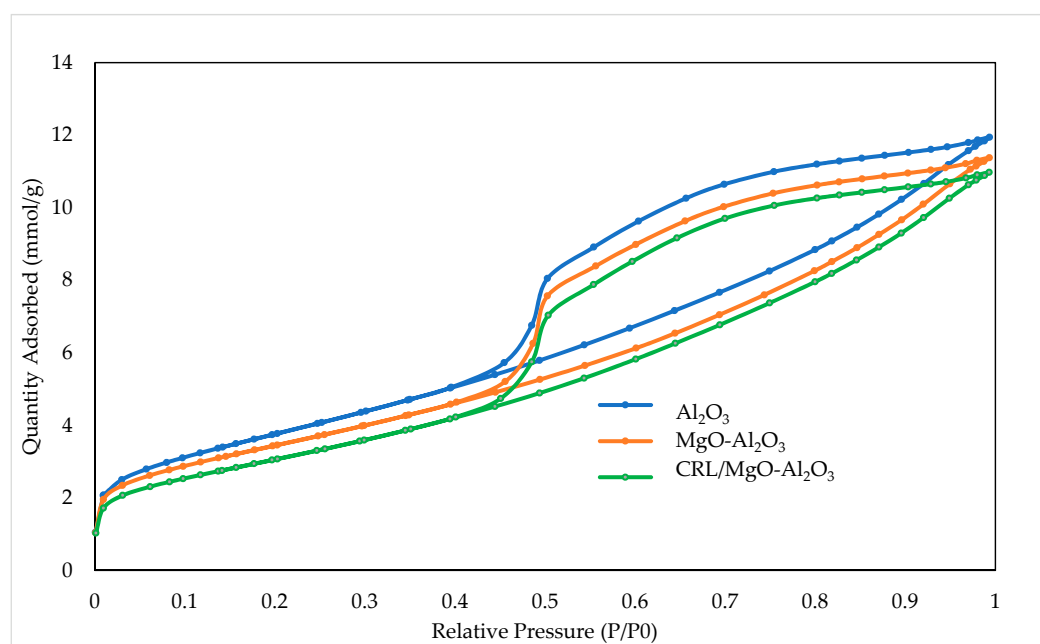


Figure 13. Nitrogen adsorption–desorption isotherms for Al_2O_3 , $\text{MgO-Al}_2\text{O}_3$, and $\text{CRL/MgO-Al}_2\text{O}_3$, respectively.

2.8. Mechanisms of CRL Adsorption on $\text{MgO-Al}_2\text{O}_3$

The possible lipase adsorption mechanism was proposed based on the result analysis of FTIR and zeta potential. The surface charge of the metal oxides depends on the pH of a system due to the presence of the hydroxyl group that may protonate or deprotonate, depending on the pH of the contact solution. At pHs above the isoelectric point (pI), the compound will be negatively charged and deprotonate and, therefore, adsorb cations strongly [78]. The same concept applies to protein, in which the protein is positively charged at a pH below pI and negatively charged at a pH above pI [79]. The pI of $\text{MgO-Al}_2\text{O}_3$ is 8.10; on the other hand, the pI of CRL is 5.2. In the immobilization medium (pH 7), the $\text{MgO-Al}_2\text{O}_3$ is positively charged, while CRL possessed a negative charge. Hence, the

electrostatic interaction between the negatively charged CRL and the positively charged hydroxyl groups on the support increases the amount of CRL adsorption. Meanwhile, the pI for Al_2O_3 is 3.71, which was negatively charged at pH 7, causing electrostatic repulsion of CRL on the support, thus, decreasing adsorption efficiency of CRL on the untreated support. The mechanisms of CRL adsorption on $\text{MgO-Al}_2\text{O}_3$ at pH 7 are illustrated in Figure 14.

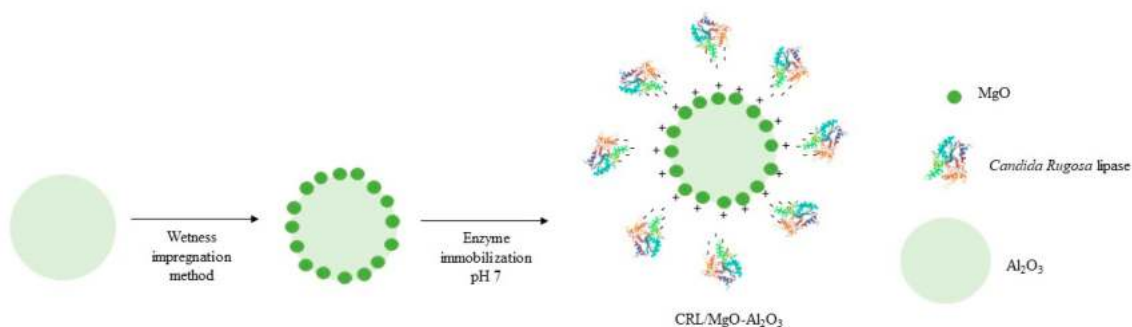


Figure 14. The mechanisms of CRL adsorption on $\text{MgO-Al}_2\text{O}_3$ at pH 7.

2.9. Application of CRL/ $\text{MgO-Al}_2\text{O}_3$ for Biodiesel Production

Lastly, the CRL/ $\text{MgO-Al}_2\text{O}_3$ was employed for biodiesel production via a transesterification reaction using methanol. The FAME yield using CRL/ $\text{MgO-Al}_2\text{O}_3$ biocatalyst was compared with $\text{MgO-Al}_2\text{O}_3$ and free CRL, as tabulated in Table 7.

Table 7. Biodiesel production using free CRL, $\text{MgO-Al}_2\text{O}_3$, and CRL- $\text{MgO-Al}_2\text{O}_3$, respectively.

Catalyst	Biodiesel Yield (%)	Mass Conversion (%)
Free CRL	48.10	86.00
$\text{MgO-Al}_2\text{O}_3$	23.00	80.90
CRL/ $\text{MgO-Al}_2\text{O}_3$	59.91	90.90

The result shows that CRL/ $\text{MgO-Al}_2\text{O}_3$ produced the highest mass conversion, up to 90.90%, corresponding to 59.91% of biodiesel yield as compared to free CRL and $\text{MgO-Al}_2\text{O}_3$ with 86.00% and 80.87% mass conversion attributed to 48.1% and 23.0% of biodiesel yield, respectively. Costa et al. reported a mass conversion of 89.7%, which corresponds to 57.3% of biodiesel yield obtained from enzymatic transesterification of *Crambe abyssinica* [7]. The higher biodiesel yield of CRL/ $\text{MgO-Al}_2\text{O}_3$ may be attributed to the dual-active site of $\text{MgO-Al}_2\text{O}_3$ and immobilized CRL that served as a chemoenzymatic catalyst. In this project, the $\text{MgO-Al}_2\text{O}_3$ successfully delivered in its role as a support for CRL immobilization while performing its catalytic efficiency as a chemical catalyst. The low biodiesel yield for $\text{MgO-Al}_2\text{O}_3$, compared to a study conducted by Ashok et al., may be attributed to the low reaction temperature used in this study [28]. Since lipases are less tolerant and prompt to denaturation at high reaction temperatures, 50 °C was chosen in this study. Meanwhile, low biodiesel yield for free CRL may be because of methanol inhibition during the transesterification reaction, which can be overcome using CRL/ $\text{MgO-Al}_2\text{O}_3$ [80]. CRL/ $\text{MgO-Al}_2\text{O}_3$ may be able to protect the lipase from structural changes and denaturation due to methanol addition. Magnesium oxide could incorporate to form a stable molecular structure of protein and resist any conformational changes due to the presence of methanol [81]. The optimization of different parameters (temperature, oil-to-methanol ratio, agitation speed, catalyst loading, and time) for biodiesel production should be evaluated to properly address the effect of these parameters towards a chemoenzymatic reaction.

3. Materials and Methods

3.1. Enzyme and Chemicals

Commercial lipase from *Candida rugosa* (≥ 700 U/mg), 3 mm alumina beads (Al_2O_3), magnesium nitrate hexahydrate ($\text{Mg}(\text{NO}_2)_3 \cdot 6\text{H}_2\text{O}$), calcium nitrate tetrahydrate ($\text{Ca}(\text{NO}_2)_3 \cdot 4\text{H}_2\text{O}$), *p*-nitrophenyl palmitate (*p*-NPP), and sodium deoxycholate were purchased from Sigma-Aldrich, Germany. Meanwhile, Triton X-100 and Arabic gum were obtained from R&M Chemicals. Copper (II) nitrate tetrahydrate ($\text{Cu}(\text{NO}_2)_3 \cdot 3\text{H}_2\text{O}$), zinc nitrate hexahydrate ($\text{Zn}(\text{NO}_2)_3 \cdot 6\text{H}_2\text{O}$), and nickel nitrate hexahydrate ($\text{Ni}(\text{NO}_2)_3 \cdot 6\text{H}_2\text{O}$) were obtained from Qrec.

3.2. Preparation of MO- Al_2O_3 Support

Wetness impregnation method was performed by immersing 5 g of Al_2O_3 into respective amount of metal precursor until it was evenly absorbed on the support's surface. This support was called MO- Al_2O_3 . Then, MO- Al_2O_3 was filtered and aged at 60–70 °C overnight prior to calcination at 300 °C for 1 h. Next, CRL was immobilized on the MO- Al_2O_3 support using 1 g of support in 2 g/L of CRL concentration for 3 h under 100 rpm agitation speed. Enzyme solution was prepared by dissolving CRL in phosphate buffer (0.1 M, pH 7). The beads were filtered and washed after immobilization procedure using phosphate buffer to remove unbound and non-specific lipase. The washing solutions were collected during the immobilization procedure to determine the amount of residual lipase using Bradford method. The immobilization efficiency of lipase onto MgO- Al_2O_3 was calculated according to Xie and Huang [43].

3.3. Determination of Lipase Activity

The enzymatic activity of free and immobilized lipase was determined followed by a modified method of Winkler and Stuckmann [82], using *p*-NPP as a substrate and spectrophotometric detection of the released *p*-nitrophenol (*p*-NP) at 410 nm. One enzyme unit is defined as the amount of enzyme that liberates 1 μmol of *p*-nitrophenol (*p*-NP) per minute per mL under assay conditions.

3.4. Experimental Design for Response Surface Methodology (RSM) and Statistical Analysis

The experimental design was developed via Box–Behnken Design (BBD) using Design-Expert version 11 to optimize the immobilization conditions. The experimental design consists of 5 parameters which are agitation speed (50–150 rpm), CRL concentration (1–4 g/L), temperature (20–40 °C), time (2–6 h), and weight of MgO- Al_2O_3 beads (1–3 g). The central point repeats are required since they allow for the estimate of pure experimental errors and the verification of the model's fit. [32]. After entering the ranges for the parameter, a design that consisted of 43 experimental runs, including replicates at the central point, was suggested and the results of the predicted and experimental value for activity recovery and immobilization yield. The regression analysis of the experimental data and response surfaces was performed using analysis of variance (ANOVA).

3.5. Biochemical Characterization of Free CRL and Hybrid CRL/MgO- Al_2O_3

Biochemical characterization of the free CRL and hybrid CRL/MgO- Al_2O_3 included heat stability, pH stability, mechanical stability, leaching analysis, reusability, and solvent tolerance analysis. The optimum conditions for their activity were also determined. Thermal stability of free and CRL/MgO- Al_2O_3 was identified by measuring residual activity after 75 min of incubation in sodium phosphate buffer at temperatures ranging from 40 to 70 °C (0.1 M, pH 7). The pH stability of free CRL and hybrid CRL/MgO- Al_2O_3 was determined by evaluating residual activity after incubation at different pH buffers ranging from pH 4 to 10 for 60 min at 40 °C. The buffers used were 0.05 M sodium acetate buffer (pH 4 and 5), 0.05 M potassium phosphate buffer (pH 6, 7, and 8), 0.05 M Tris-HCl buffer (pH 9), and 0.5 M Glycine-NaOH buffer (pH 10 and 11). The residual CRL activity was subsequently determined by *p*-NPP assay and was calculated relative to the initial activity before incubation. The influence of temperature on CRL activity was investigated using

an enzyme assay at various temperatures (10–80 °C) and the influence of pH on enzyme activity was examined by employing a buffer solution with varying pH values (pH 4–10) in an enzyme experiment. The relative activity of CRL at different temperatures and pHs was calculated as a relative activity. The highest activity of free CRL and CRL/MgO-Al₂O₃ was defined as 100% relative activity.

Mechanical stability of free CRL and hybrid CRL/MgO-Al₂O₃ was determined by measuring residual activity after 60 min of shaking at 30 °C at various rotating speeds in an orbital shaker (50 rpm, 100 rpm, 150 rpm, 200 rpm, and 250 rpm). *p*-NPP assay was used to determine the residual CRL activity, which was computed relative to the original activity before shaking. The starting activity level was set to 100%. The *p*-NPP assay was used to determine the CRL activity in the supernatant. At 37 °C, the reusability of all enzyme preparations was assessed. The enzyme was rinsed with potassium phosphate buffer after each test cycle (0.1 M, pH 7). Then, a fresh reaction mixture was added. The CRL activity of each cycle was measured in terms of residual activity. Free CRL and CRL/MgO-Al₂O₃ activity of the first cycle was set as 100%. Next, CRL/MgO-Al₂O₃ and free CRL were incubated in 1 mL of 5%, 10%, 20%, 30%, 40%, and 50% (*v/v*) of ethanol, isopropanol, methanol, and tert-butanol for 30 min. Then, the lipase assay was performed and the residual activity was calculated based on initial activity before addition of solvent.

3.6. Physical Characterization of Support (MgO-Al₂O₃) and CRL/MgO-Al₂O₃

The estimation of purity of the prepared biocatalysts and the magnesium composition were determined by inductively coupled plasma optical emission spectroscopy (ICP-OES) using an Optical Emission Spectrometer Avio™ 200. Prior to elemental analysis, the solid sample was digested using Microwave Digester Titan MPS to break down the sample.

The degradation of biocatalysts was studied utilizing a Netzsch simultaneous thermal analyzer STA409 PC and thermogravimetric analysis (TGA) with simultaneous differential thermal analysis (DTA). The temperature accuracy of the instrument was calibrated using the melting points of a series of metal standards, resulting in a temperature accuracy of 1 °C. In several experiments, samples of 20–30 mg were heated in alumina crucibles from room temperature to 1490 °C with heating speeds ranging from 5 to 40 °C/min and oxygen flow rates of 50 mL/min.

The Fourier transform infrared spectroscopy (FTIR) was performed using a Shimadzu IRTracer-100, for the support and immobilized catalyst in order to check the functional group changes on Al₂O₃ after wetness impregnation and CRL immobilization. The surface morphology of the catalyst was obtained using field emission scanning electron microscopy (FESEM) Hitachi SU 8020. The sample was attached by carbon tape on special platform called stub, coated with platinum using a platinum sputter at 10⁻¹ Mbar using a Bio Rad Polaron Division SEM coating system machine. The sample was covered with a tungsten filament using an electron gun under 25 kV resolutions to obtain the required magnification image. The images were observed at different points along the platform.

The nitrogen adsorption–desorption isotherms of the support and immobilized enzyme were measured on a Micromeritics TriStar II device at −196.15 °C. All samples were degassed at either 150 or 250 °C in vacuum for 8 h prior to the analysis. The specific surface area was determined by Brunnauer, Emmett, and Teller (BET) method for adsorption data in relative pressure range from 0.05 to 0.20. The pore volumes were calculated from the quantity of nitrogen adsorbed at a relative pressure of 0.97. Average pore diameters were determined from the nitrogen desorption branch according to Barrett–Joyner–Halenda (BJH). The zeta potential of the CRL and support was analyzed using Malvern Zetasizer Nano ZSP.

3.7. Biodiesel Production and Analysis of FAME Content

CRL/MgO-Al₂O₃ was employed for transesterification of waste cooking oil to biodiesel using methanol. The acid value for waste cooking oil was recorded as 10.51 (mg KOH/g fat) and 4.79% of FFA content. The free fatty acid compositions of waste cooking oil are palmitic

acid ($42.75\% \pm 1.80$), stearic acid ($5.25\% \pm 0.25$), oleic acid ($40.84\% \pm 3.65$), and linoleic acid ($8.35\% \pm 0.60$). The transesterification reaction was performed under these conditions: catalyst loading ($3\% w/w$), temperature $50\text{ }^{\circ}\text{C}$, reaction time (48 h), oil-to-methanol molar ratio ($1:12 w/w$), water content ($2\% w/w$), and agitation speed at 250 rpm. Free CRL (0.0006 mg) was used as a reference to analyse the efficiency of immobilised enzyme. The amount of free CRL represents the amount of CRL that was adsorbed on the $\text{MgO-Al}_2\text{O}_3$. Next, the fatty acid methyl ester (FAME) content in the reaction mixture will be quantified using a gas chromatography-flame ionization detector (GC-FID), equipped with an HP-INNOWax column ($30\text{ m} \times 0.25\text{ mm} \times 0.25\text{ }\mu\text{m}$) and nitrogen was used as a carrier gas. The sample weighed approximately 0.025 g and was added into the vials followed by the addition of 0.5 mL of 0.01 g/mL methyl heptadecanoate as internal standard. The oven temperature of gas chromatography was set at $250\text{ }^{\circ}\text{C}$. The initial temperature of the column was programmed at $60\text{ }^{\circ}\text{C}$ for 2 min with the first ramp rate of $10\text{ }^{\circ}\text{C}/\text{min}$ up to $200\text{ }^{\circ}\text{C}$. The second ramp was programmed at $5\text{ }^{\circ}\text{C}/\text{min}$ for 2 min to $240\text{ }^{\circ}\text{C}$ and hold for 7 min. The injector and detector temperatures was set up at $250\text{ }^{\circ}\text{C}$ and the gas flow rate was $1\text{ mL}/\text{min}$. The FAMFAME purity, mass conversion, and biodiesel yield are calculated using Equations (3)–(5).

$$\text{FAME Purity (\%)} = \frac{(\sum A - \sum \text{AEI})}{\sum \text{AEI}} \times \frac{\text{CEI} * \text{VEI}}{m} \times 100 \quad (3)$$

where:

$\sum A$ = total peak area from the FAME C14:0 to C24:1

AEI = peak area of methyl heptadecanoate

CEI = concentration, in mg/mL , of the methyl heptadecanoate solution

VEI = volume, in mL , of the methyl heptadecanoate solution

m = mass, in mg , of the sample

The mass conversion was calculated taking into consideration the amount of raw material used in the transesterification reaction and the final weight of the biodiesel, as described in Equation (4) [7].

$$\text{Mass conversion (\%)} = \frac{\text{Weight of oil after transesterification} *}{\text{Weight of raw oil}} * 100 \quad (4)$$

$$\text{Biodiesel yield (\%)} = \frac{\text{Mass conversion} * \text{purity of FAME}}{100} \quad (5)$$

4. Conclusions

$\text{MgO-Al}_2\text{O}_3$ was successfully prepared via wetness an impregnation and calcination method to be used for lipase immobilization via electrostatic interaction. The addition of MgO onto Al_2O_3 successfully changed the surface charge in the support and subsequently enhanced the electrostatic interaction between the negatively charged CRL and the positively charged hydroxyl groups on the support. The subsequent analysis of variance (ANOVA) showed that immobilization of lipase was most suitably described with a linear model due to its highest-order polynomial with the significance of additional terms and the model was not aliased. The optimized conditions for activity recovery and immobilization efficiency were obtained as follows: 121.53 rpm agitation speed, 2.84 g/L CRL concentration, $26.96\text{ }^{\circ}\text{C}$ temperature, 4.08 h immobilization time, and 2.69 g of $\text{MgO-Al}_2\text{O}_3$ beads. These conditions resulted in 70.5% activity recovery and 65.1% immobilization efficiency of the lipase. The reusability of immobilized CRL successfully preserved its activity to 32.7% after 12 cycles of reactions. This study explores the potential applicability of immobilized lipase in a reaction that involved solvent and is of immense interest in biodiesel application. The synthesizing of inorganic metal hybrid support for lipase immobilization can serve as a chemoenzymatic catalyst for biodiesel applications with 59.90% of biodiesel yield.

Further optimization studies focusing on the parameters affecting biodiesel production should be conducted to produce biodiesel at the highest yield.

Supplementary Materials: The following supporting information can be downloaded at: <https://www.mdpi.com/article/10.3390/catal12080854/s1>.

Author Contributions: Conceptualization, supervision, N.I.W.A., S.T. and R.M.I.; methodology, N.N.R.; software, N.N.R.; data curation, N.N.R.; formal analysis, N.N.R.; writing—original draft preparation, N.N.R.; validation, R.A.R. and N.H.A.M.; writing—review and editing, N.N.R., N.I.W.A., S.T. and R.S.; funding acquisition, R.A.A. and N.I.W.A. All authors have read and agreed to the published version of the manuscript.

Funding: This study acknowledges the Ministry of Education (MOE) Malaysia through Fundamental Research Grant Scheme (FRGS/1/2020/TK0/UTM/02/8) for the financial support and Universiti Teknologi Malaysia (UTM) for the facilities support. The APC was funded by INTI International University Research Fund.

Conflicts of Interest: The authors declare no conflict of interest. The funders had no role in the design of the study; in the collection, analyses, or interpretation of data; in the writing of the manuscript; or in the decision to publish the results.

References

1. Gandhi, N.N.; Patil, N.S.; Sawant, S.B.; Joshi, J.B.; Wangikar, P.P.; Mukesh, D. Lipase-Catalyzed Esterification. *Catal. Rev.* **2007**, *42*, 439–480. [[CrossRef](#)]
2. Ishak, S.N.H.; Masomian, M.; Kamarudin, N.H.A.; Ali, M.S.M.; Leow, T.C.; Rahman, R. Changes of Thermostability, Organic Solvent, and pH Stability in *Geobacillus zalihae* HT1 and Its Mutant by Calcium Ion. *Int. J. Mol. Sci.* **2019**, *20*, 2561. [[CrossRef](#)] [[PubMed](#)]
3. Pinto Brito, M.J.; Bauer, L.C.; Flores Santos, M.P.; Santos, L.S.; Ferreira Bonomo, R.C.; da Costa Ilhéu Fontan, R.; Veloso, C.M. Lipase immobilization on activated and functionalized carbon for the aroma ester synthesis. *Microporous Mesoporous Mater.* **2020**, *309*, 110576. [[CrossRef](#)]
4. Chauhan, M.; Chauhan, R.S.; Garlapati, V.K. Evaluation of a New Lipase from *Staphylococcus* sp. for Detergent Additive Capability. *BioMed Res. Int.* **2013**, *2013*, 374967. [[CrossRef](#)] [[PubMed](#)]
5. Hou, A.; Liang, L.; Du, J.; Yan, J.; Peng, B. Evaluation of lipases properties and degreasing effects in leather manufacture. In Proceedings of the 31st IULTCS Congress, Valencia, Spain, 28–30 September 2011.
6. Sarac, N.; Ugur, A. A green alternative for oily wastewater treatment: Lipase from *Acinetobacter haemolyticus* NS02-30. *Desalination Water Treat.* **2016**, *57*, 19750–19759. [[CrossRef](#)]
7. Costa, E.; Almeida, M.F.; Alvim-Ferraz, C.; Dias, J.M. Optimization of *Crambe abyssinica* enzymatic transesterification using response surface methodology. *Renew. Energy* **2021**, *174*, 444–452. [[CrossRef](#)]
8. Ramlee, N.N.; Md Ilias, R.; Toemen, S.; Abdul Manas, N.H.; Wan Azelee, N.I. Esterification of a waste cooking oil using metal-hybrid catalysts for chemoenzymatic reactions. *Mater. Today Proc.* **2021**, *47*, 1280–1286. [[CrossRef](#)]
9. Lyu, X.; Gonzalez, R.; Horton, A.; Li, T. Immobilization of Enzymes by Polymeric Materials. *Catalysts* **2021**, *11*, 1211. [[CrossRef](#)]
10. Rueda, N.; dos Santos, C.S.; Rodriguez, M.D.; Albuquerque, T.L.; Barbosa, O.; Torres, R.; Ortiz, C.; Fernandez-Lafuente, R. Reversible immobilization of lipases on octyl-glutamic agarose beads: A mixed adsorption that reinforces enzyme immobilization. *J. Mol. Catal. B Enzym.* **2016**, *128*, 10–18. [[CrossRef](#)]
11. Sabi, G.J.; Gama, R.S.; Fernandez-Lafuente, R.; Cancino-Bernardi, J.; Mendes, A.A. Decyl esters production from soybean-based oils catalyzed by lipase immobilized on differently functionalized rice husk silica and their characterization as potential biolubricants. *Enzym. Microb. Technol.* **2022**, *157*, 110019. [[CrossRef](#)]
12. Zhou, W.; Zhuang, W.; Ge, L.; Wang, Z.; Wu, J.; Niu, H.; Liu, D.; Zhu, C.; Chen, Y.; Ying, H. Surface functionalization of graphene oxide by amino acids for *Thermomyces lanuginosus* lipase adsorption. *J. Colloid Interface Sci.* **2019**, *546*, 211–220. [[CrossRef](#)]
13. Romero Toledo, R.; Sánchez, M.B.; Porras, G.R.; Ramírez, R.F.; Pérez Larios, A.; Ramirez, A.M.; Rosales, M.M. Effect of Mg as Impurity on the Structure of Mesoporous γ -Al₂O₃: Efficiency as Catalytic Support in HDS of DBT. *Int. J. Chem. React. Eng.* **2018**, *16*. [[CrossRef](#)]
14. Qiao, N.; Nong, Y.; Liu, N.; Liang, Y. Heterogeneous catalyst of porous anodic aluminum oxide with Al substrate supported metal nanoparticles. *Mater. Chem. Phys.* **2019**, *225*, 458–463. [[CrossRef](#)]
15. Rutkowska, I.; Marchewka, J.; Jelen, P.; Odziomek, M.; Korpys, M.; Paczkowska, J.; Sitarz, M. Chemical and Structural Characterization of Amorphous and Crystalline Alumina Obtained by Alternative Sol-Gel Preparation Routes. *Materials* **2021**, *14*, 1761. [[CrossRef](#)]
16. Mello, N.M.; Rego, A.S.C.; Brocchi, E.A.; Campos, J.B.d.; Moura, F.J.; Souza, R.F.M. Effect of an Alumina Supported Palladium Catalyst on the Magnesium Sulfate Decomposition Kinetics. *Mater. Res.* **2020**, *23*. [[CrossRef](#)]
17. Coutinho, T.C.; Tardioli, P.W.; Farinas, C.S. Hydroxyapatite nanoparticles modified with metal ions for xylanase immobilization. *Int. J. Biol. Macromol.* **2020**, *150*, 344–353. [[CrossRef](#)]

18. Wang, B.; Xiong, X.; Ren, H.; Huang, Z. Preparation of MgO nanocrystals and catalytic mechanism on phenol ozonation. *RSC Adv.* **2017**, *7*, 43464–43473. [[CrossRef](#)]
19. Mulcahy, F.M.; Houalla, M.; Hercules, D.M. The Effect of The Isoelectric Point on The Adsorption on Molybdates on Fluoride-Modified Alumina. *J. Catal.* **1987**, *106*, 210–215. [[CrossRef](#)]
20. Satyawali, Y.; Roy, S.V.; Roevens, A.; Meynen, V.; Mullens, S.; Jochems, P.; Doyen, W.; Cauwenberghs, L.; Dejonghe, W. Characterization and analysis of the adsorption immobilization mechanism of β -galactosidase on metal oxide powders. *RSC Adv.* **2013**, *3*, 24054–24062. [[CrossRef](#)]
21. Eskandari, S.; Tate, G.; Leaphart, N.R.; Regalbuto, J.R. Nanoparticle Synthesis via Electrostatic Adsorption Using Incipient Wetness Impregnation. *ACS Catal.* **2018**, *8*, 10383–10391. [[CrossRef](#)]
22. Zahan, K.; Kano, M. Biodiesel Production from Palm Oil, Its By-Products, and Mill Effluent: A Review. *Energies* **2018**, *11*, 2132. [[CrossRef](#)]
23. Talha, N.S.; Sulaiman, S. Overview Of Catalyst In Biodiesel Production. *ARPN J. Eng. Appl. Sci.* **2016**, *11*, 439–442.
24. Cesarini, S.; Pastor, F.I.J.; Nielsen, P.M.; Diaz, P. Moving towards a Competitive Fully Enzymatic Biodiesel Process. *Sustainability* **2015**, *7*, 7884–7903. [[CrossRef](#)]
25. Zdarta, J.; Meyer, A.; Jesionowski, T.; Pinelo, M. A General Overview of Support Materials for Enzyme Immobilization: Characteristics, Properties, Practical Utility. *Catalysts* **2018**, *8*, 92. [[CrossRef](#)]
26. Zhong, L.; Feng, Y.; Hu, H.; Xu, J.; Wang, Z.; Du, Y.; Cui, J.; Jia, S. Enhanced enzymatic performance of immobilized lipase on metal organic frameworks with superhydrophobic coating for biodiesel production. *J. Colloid Interface Sci.* **2021**, *602*, 426–436. [[CrossRef](#)]
27. Zhong, L.; Feng, Y.; Wang, G.; Wang, Z.; Bilal, M.; Lv, H.; Jia, S.; Cui, J. Production and use of immobilized lipases in/on nanomaterials: A review from the waste to biodiesel production. *Int. J. Biol. Macromol.* **2020**, *152*, 207–222. [[CrossRef](#)] [[PubMed](#)]
28. Ashok, A.; Kennedy, L.J.; Vijaya, J.J.; Aruldoss, U. Optimization of biodiesel production from waste cooking oil by magnesium oxide nanocatalyst synthesized using coprecipitation method. *Clean Technol. Environ. Policy* **2018**, *20*, 1219–1231. [[CrossRef](#)]
29. Jing, J.-y.; Zhang, Z.-y.; Wang, S.-d.; Li, W.-y. Influence of calcination temperature on the structure and catalytic reforming performance of Ni/CaO-Al₂O₃ catalyst. *J. Fuel Chem. Technol.* **2018**, *46*, 673–679. [[CrossRef](#)]
30. Wong, Y.C.; Tan, Y.P.; Taufiq-Yap, Y.H.; Ram, I. Effect of Calcination Temperatures of CaO/Nb² Catalysts on Biodiesel Production. *Sains Malays.* **2014**, *43*, 783–790.
31. Shahedi, M.; Habibi, Z.; Yousefi, M.; Brask, J.; Mohammadi, M. Improvement of biodiesel production from palm oil by co-immobilization of *Thermomyces lanuginosa* lipase and *Candida antarctica* lipase B: Optimization using response surface methodology. *Int. J. Biol. Macromol.* **2021**, *170*, 490–502. [[CrossRef](#)] [[PubMed](#)]
32. Moreira, K.S.; Moura Júnior, L.S.; Monteiro, R.R.C.; de Oliveira, A.L.B.; Valle, C.P.; Freire, T.M.; Fachine, P.B.A.; de Souza, M.C.M.; Fernandez-Lorente, G.; Guisan, J.M.; et al. Optimization of the Production of Enzymatic Biodiesel from Residual Babassu Oil (*Orbignya* sp.) via RSM. *Catalysts* **2020**, *10*, 414. [[CrossRef](#)]
33. Jamil, N.; Man, R.C.; Suhaimi, S.; Shaarani, S.M.; Arshad, Z.I.M.; Mudalip, S.K.A.; Sulaiman, S.Z. Effect of Immobilization Parameters on the Immobilization of Cyclodextrin Glucanotransferase on Hollow Fiber Membrane. *J. Teknol.* **2019**, *82*. [[CrossRef](#)]
34. Masuda, Y.; Kugimiya, S.-i.; Kato, K. Improvement of thermal-stability of enzyme immobilized onto mesoporous zirconia. *J. Asian Ceram. Soc.* **2018**, *2*, 11–19. [[CrossRef](#)]
35. Adnan, M.; Li, K.; Xu, L.; Yan, Y. X-Shaped ZIF-8 for Immobilization *Rhizomucor miehei* Lipase via Encapsulation and Its Application toward Biodiesel Production. *Catalysts* **2018**, *8*, 96. [[CrossRef](#)]
36. Rios, N.S.; Arana-Peña, S.; Mendez-Sanchez, C.; Lokha, Y.; Cortes-Corberan, V.; Gonçalves, L.R.B.; Fernandez-Lafuente, R. Increasing the Enzyme Loading Capacity of Porous Supports by a Layer-by-Layer Immobilization Strategy Using PEI as Glue. *Catalysts* **2019**, *9*, 576. [[CrossRef](#)]
37. Fernandez-Lopez, L.; Pedrero, S.G.; Lopez-Carrobles, N.; Gorines, B.C.; Virgen-Ortiz, J.J.; Fernandez-Lafuente, R. Effect of protein load on stability of immobilized enzymes. *Enzym. Microb. Technol.* **2017**, *98*, 18–25. [[CrossRef](#)]
38. Silveira, M.H.L.; Rau, M.; Andreaus, J. Influence of mechanical agitation on the pH profile of total, soluble and insoluble filter paper activity of *Hypocrea jecorina* cellulase preparations. *Biocatal. Biotransformation* **2012**, *30*, 63–70. [[CrossRef](#)]
39. Chang, S.-F.; Chang, S.-W.; Yen, Y.-H.; Shieh, C.-J. Optimum immobilization of *Candida rugosa* lipase on Celite by RSM. *Appl. Clay Sci.* **2007**, *37*, 67–73. [[CrossRef](#)]
40. Andriano Jospin, D. Optimum Immobilization of *Candida antartica* B Lipase on Natural Silica by RSM. *Am. J. Chem. Eng.* **2017**, *5*, 43–48. [[CrossRef](#)]
41. Yu, D.; Zhang, X.; Wang, T.; Geng, H.; Wang, L.; Jiang, L.; Elfalleh, W. Immobilized *Candida antarctica* lipase B (CALB) on functionalized MCM-41: Stability and catalysis of transesterification of soybean oil and phytoesterol. *Food Biosci.* **2021**, *40*, 100906. [[CrossRef](#)]
42. Rana, S.; Sharma, A.; Kumar, A.; Kanwar, S.S.; Singh, M. Utility of Silane-Modified Magnesium-Based Magnetic Nanoparticles for Efficient Immobilization of *Bacillus thermoamylovorans* Lipase. *Appl. Biochem. Biotechnol.* **2020**, *192*, 1029–1043. [[CrossRef](#)]
43. Xie, W.; Huang, M. Immobilization of *Candida rugosa* lipase onto graphene oxide Fe₃O₄ nanocomposite characterization and application for biodiesel production. *Energy Convers. Manag.* **2018**, *159*, 42–53. [[CrossRef](#)]
44. Morrell, R. *Handbook of Properties of Technical Engineering Ceramics*; Her Majesty's Stationery Office: London, UK, 1989.
45. Cui, J.D.; Liu, R.L.; Li, L.B. A facile technique to prepare cross-linked enzyme aggregates of bovine pancreatic lipase using bovine serum albumin as an additive. *Korean J. Chem. Eng.* **2016**, *33*, 610–615. [[CrossRef](#)]

46. Cao, L. *Carrier-Bound Immobilized Enzymes: Principles, Application and Design*; Wiley-VCH Verlag GmbH & Co. KGaA: Weinheim, Germany, 2005. [[CrossRef](#)]
47. Bussamara, R.; Dall'agnol, L.; Schrank, A.; Fernandes, K.F.; Vainstein, M.H. Optimal Conditions for Continuous Immobilization of *Pseudozyma hubeiensis* (Strain HB85A) Lipase by Adsorption in a Packed-Bed Reactor by Response Surface Methodology. *Enzym. Res.* **2012**, *2012*, 329178. [[CrossRef](#)]
48. George, R.; Sugunan, S. Kinetics of adsorption of lipase onto different mesoporous materials: Evaluation of Avrami model and leaching studies. *J. Mol. Catal. B Enzym.* **2014**, *105*, 26–32. [[CrossRef](#)]
49. Costantini, A.; Califano, V. Lipase Immobilization in Mesoporous Silica Nanoparticles for Biofuel Production. *Catalysts* **2021**, *11*, 629. [[CrossRef](#)]
50. Jafarian, F.; Bordbar, A.K.; Zare, A.; Khosropour, A. The performance of immobilized *Candida rugosa* lipase on various surface modified graphene oxide nanosheets. *Int. J. Biol. Macromol.* **2018**, *111*, 1166–1174. [[CrossRef](#)]
51. Gürdaş, S.; Güleç, H.A.; Mutlu, M. Immobilization of *Aspergillus oryzae* β -Galactosidase onto Duolite A568 Resin via Simple Adsorption Mechanism. *Food Bioprocess Technol.* **2010**, *5*, 904–911. [[CrossRef](#)]
52. Virgen-Ortiz, J.J.; Pedrero, S.G.; Fernandez-Lopez, L.; Lopez-Carrobles, N.; Gorines, B.C.; Otero, C.; Fernandez-Lafuente, R. Desorption of Lipases Immobilized on Octyl-Agarose Beads and Coated with Ionic Polymers after Thermal Inactivation. Stronger Adsorption of Polymers/Unfolded Protein Composites. *Molecules* **2017**, *22*, 91. [[CrossRef](#)]
53. Amini, Z.; Ong, H.C.; Harrison, M.D.; Kusumo, F.; Mazaheri, H.; Ilham, Z. Biodiesel production by lipase-catalyzed transesterification of *Ocimum basilicum* L. (sweet basil) seed oil. *Energy Convers. Manag.* **2017**, *132*, 82–90. [[CrossRef](#)]
54. Zare, A.; Bordbar, A.K.; Razmjou, A.; Jafarian, F. The immobilization of *Candida rugosa* lipase on the modified polyethersulfone with MOF nanoparticles as an excellent performance bioreactor membrane. *J. Biotechnol.* **2019**, *289*, 55–63. [[CrossRef](#)] [[PubMed](#)]
55. Cea, M.; González, M.E.; Abarzúa, M.; Navia, R. Enzymatic esterification of oleic acid by *Candida rugosa* lipase immobilized onto biochar. *J. Environ. Manag.* **2019**, *242*, 171–177. [[CrossRef](#)] [[PubMed](#)]
56. Cao, S.L.; Huang, Y.M.; Li, X.H.; Xu, P.; Wu, H.; Li, N.; Lou, W.Y.; Zong, M.H. Preparation and Characterization of Immobilized Lipase from *Pseudomonas Cepacia* onto Magnetic Cellulose Nanocrystals. *Sci. Rep.* **2016**, *6*, 20420. [[CrossRef](#)]
57. Badoei-Dalfard, A.; Shahba, A.; Zaare, F.; Sargazi, G.; Seyedalipour, B.; Karami, Z. Lipase immobilization on a novel class of Zr-MOF/electrospun nanofibrous polymers: Biochemical characterization and efficient biodiesel production. *Int. J. Biol. Macromol.* **2021**, *192*, 1292–1303. [[CrossRef](#)] [[PubMed](#)]
58. Pulido, I.Y.; Prieto, E.; Jimenez-Junca, C. Ethanol as additive enhance the performance of immobilized lipase LipA from *Pseudomonas aeruginosa* on polypropylene support. *Biotechnol. Rep.* **2021**, *31*, e00659. [[CrossRef](#)]
59. Kamal, M.Z.; Yedavalli, P.; Deshmukh, M.V.; Rao, N.M. Lipase in aqueous-polar organic solvents: Activity, structure, and stability. *Protein Sci.* **2013**, *22*, 904–915. [[CrossRef](#)]
60. Ballal, D.; Chapman, W.G. Hydrophobic and hydrophilic interactions in aqueous mixtures of alcohols at a hydrophobic surface. *J. Chem. Phys.* **2013**, *139*, 114706. [[CrossRef](#)] [[PubMed](#)]
61. Ycel, S.; Terziolu, P.; Zime, D. Lipase Applications in Biodiesel Production. In *Biodiesel—Feedstocks, Production and Applications*; Intech Open: London, UK, 2012. [[CrossRef](#)]
62. Fu, B.; Vasudevan, P.T. Effect of Solvent–Co-solvent Mixtures on Lipase-Catalyzed Transesterification of Canola Oil. *Energy Fuels* **2010**, *24*, 4646–4651. [[CrossRef](#)]
63. Sousa, R.R.; Silva, A.S.A.; Fernandez-Lafuente, R.; Ferreira-Leitão, V.S. Solvent-free esterifications mediated by immobilized lipases: A review from thermodynamic and kinetic perspectives. *Catal. Sci. Technol.* **2021**, *11*, 5696–5711. [[CrossRef](#)]
64. Islam, M.A.; Chowdhury, M.A.; Shuvho, M.B.A.; Aziz, M.A.; Kchaou, M. Thermal analysis of hybrid composites reinforced with Al₂O₃ and SiO₂ filler particles. *Mater. Res. Express* **2020**, *6*, 125361. [[CrossRef](#)]
65. Asmat, S.; Husain, Q.; Khan, M.S. A polypyrrole–methyl anthranilate functionalized worm-like titanium dioxide nanocomposite as an innovative tool for immobilization of lipase: Preparation, activity, stability and molecular docking investigations. *N. J. Chem.* **2018**, *42*, 91–102. [[CrossRef](#)]
66. Sulaiman, N.F.; Hashim, A.N.N.; Toemen, S.; Rosid, S.J.M.; Mokhtar, W.N.A.W.; Nadarajan, R.; Bakar, W.A.W.A. Biodiesel production from refined used cooking oil using co-metal oxide catalyzed transesterification. *Renew. Energy* **2020**, *153*, 1–11. [[CrossRef](#)]
67. Li, Q.; Chen, Y.; Bai, S.; Shao, X.; Jiang, L.; Li, Q. Immobilized lipase in bio-based metal-organic frameworks constructed by biomimetic mineralization: A sustainable biocatalyst for biodiesel synthesis. *Colloids Surf. B Biointerface* **2020**, *188*, 110812. [[CrossRef](#)]
68. Patel, V.; Shah, C.; Deshpande, M.; Madamwar, D. Zinc Oxide Nanoparticles Supported Lipase Immobilization for Bio-transformation in Organic Solvents: A Facile Synthesis of Geranyl Acetate, Effect of Operative Variables and Kinetic Study. *Appl. Biochem. Biotechnol.* **2016**, *178*, 1630–1651. [[CrossRef](#)] [[PubMed](#)]
69. Toledo, R.R.; Santoyo, V.R.; Sánchez, D.M.; Rosales, M.M. Effect of aluminum precursor on physicochemical properties of Al₂O₃ by hydrolysis/precipitation method. *Nova Sci.* **2018**, *10*, 83–89. [[CrossRef](#)]
70. Zhang, L.; Wu, Y.; Zhang, L.; Wang, Y.; Li, M. Synthesis and characterization of mesoporous alumina with high specific area via coprecipitation method. *Vacuum* **2016**, *133*, 1–6. [[CrossRef](#)]
71. Panasyuk, G.P.; Azarova, L.A.; Belan, V.N.; Semenov, E.A.; Danchevskaya, M.N.; Voroshilov, I.L.; Kozerozhets, I.V.; Pershikov, S.A.; Kharatyan, S.Y. Methods for High-Purity Aluminum Oxide Production for Growth of Leucosapphire Crystals (Review). *Theor. Found. Chem. Eng.* **2019**, *53*, 596–601. [[CrossRef](#)]

72. Wang, J.; Lia, K.; He, Y.; Wang, Y.; Han, X.; Yan, Y. Enhanced performance of lipase immobilized onto Co^{2+} -chelated magnetic nanoparticles and its application in biodiesel production. *Fuel* **2019**, *255*, 115794. [[CrossRef](#)]
73. Nematian, T.; Shakeri, A.; Salehi, Z.; Saboury, A.A. Lipase immobilized on functionalized superparamagnetic few-layer graphene oxide as an efficient nanobiocatalyst for biodiesel production from *Chlorella vulgaris* bio-oil. *Biotechnol Biofuels* **2020**, *13*, 57. [[CrossRef](#)] [[PubMed](#)]
74. Harun, Z.; Ismail, N.F.; Badarulzaman, N.A. Effect of MgO Additive on Microstructure of Al_2O_3 . *Adv. Mater. Res.* **2012**, *488–489*, 335–339. [[CrossRef](#)]
75. Alothman, Z. A Review: Fundamental Aspects of Silicate Mesoporous Materials. *Materials* **2012**, *5*, 2874–2902. [[CrossRef](#)]
76. Mahlambi, M.M.; Mishra, A.K.; Mishra, S.B.; Krause, R.W.; Mamba, B.B.; Raichur, A.M. Synthesis and characterization of carbon-covered alumina (CCA) supported TiO_2 nanocatalysts with enhanced visible light photodegradation of Rhodamine B. *J. Nanoparticle Res.* **2012**, *14*, 88–89. [[CrossRef](#)]
77. Weber, S.; Abel, K.L.; Zimmermann, R.T.; Huang, X.; Bremer, J.; Rihko-Struckmann, L.K.; Batey, D.; Cipiccia, S.; Titus, J.; Poppitz, D.; et al. Porosity and Structure of Hierarchically Porous Ni/ Al_2O_3 Catalysts for CO_2 Methanation. *Catalysts* **2020**, *10*, 1471. [[CrossRef](#)]
78. Farooq, M.; Ramli, A. *The Determination of Point Zero Charge (PZC) of Al_2O_3 -MgO Mixed Oxides*; IEEE: Perak, Malaysia, 2011.
79. Zhou, G.; Chen, Y.; Yang, S. Comparative studies on catalytic properties of immobilized *Candida rugosa* lipase in ordered mesoporous rod-like silica and vesicle-like silica. *Microporous Mesoporous Mater.* **2009**, *119*, 223–229. [[CrossRef](#)]
80. Lotti, M.; Pleiss, J.; Valero, F.; Ferrer, P. Effects of methanol on lipases: Molecular, kinetic and process issues in the production of biodiesel. *Biotechnol. J.* **2015**, *10*, 22–30. [[CrossRef](#)] [[PubMed](#)]
81. Lu, J.; Deng, L.; Zhao, R.; Zhang, R.; Wang, F.; Tan, T. Pretreatment of immobilized *Candida* sp. 99–125 lipase to improve its methanol tolerance for biodiesel production. *J. Mol. Catal. B Enzym.* **2010**, *62*, 15–18. [[CrossRef](#)]
82. Winkler, U.K.; Stuckmann, M. Glycogen, Hyaluronate, and Some Other Polysaccharides Greatly Enhance the Formation of Exolipase by *Serratia marcescens*. *J. Bacteriol.* **1979**, *138*, 663–670. [[CrossRef](#)] [[PubMed](#)]